# CONTRIBUTIONS OF LAKE-EFFECT PERIOD PRECIPITATION TO THE HYDROCLIMATE OF THE GREAT SALT LAKE BASIN

by

Kristen Noelle Yeager

A thesis submitted to the faculty of
The University of Utah
in partial fulfillment of the requirements for the degree of

Master of Science

Department of Atmospheric Sciences

The University of Utah

May 2012

**STATEMENT OF THESIS APPROVAL**

The thesis of **Kristen Noelle Yeager**

has been approved by the following supervisory committee members:

| | | |
|---|---|---|
| **W. James Steenburgh** | , Chair | **3/29/2012** Date Approved |
| **John Horel** | , Member | **3/29/2012** Date Approved |
| **Andrew W. Wood** | , Member | **3/29/2012** Date Approved |

and by **Kevin Perry** , Chair of the Department of **Atmospheric Sciences**

and by Charles A. Wight, Dean of The Graduate School.

ABSTRACT

This study examines the contribution of lake-effect precipitation to the cool-season (16 Sep – 15 May) hydroclimate of the Great Salt Lake basin. Lake-effect periods are identified based on the visual inspection of KMTX radar reflectivity imagery. Quantitative lake-effect period precipitation estimates are generated using high temporal resolution radar-derived precipitation estimates to disaggregate daily COOP and SNOTEL precipitation gauge observations. This preserves the daily precipitation gauge totals and enables the separation of accumulated precipitation into lake-effect and non-lake-effect periods. Evaluation of the method at two stations (Salt Lake City International Airport and Alta-Collins) demonstrates that the method works well for estimating climatological lake-effect period totals, with some random error in hourly estimates.

Accumulated precipitation from 128 lake-effect periods indicates that Great Salt Lake-effect period precipitation contributes modestly (8.4% or less) to the cool-season precipitation of the Great Salt Lake basin with the largest contributions to the south and east of the Great Salt Lake. Lake-effect period contributions are highly variable from cool-season to cool-season and are dominated by intense episodic lake-effect periods.

The most lake-effect period precipitation falls in the months of Oct and Nov. Lake-effect period precipitation also reaches a maximum when the 700-hPa wind is between 300-360°, corresponding to the longest fetch across the Great Salt Lake.

Additional comparisons between lake-effect period precipitation and associated hydrologic and synoptic features reveal little correlation and may indicate that the sample size for a 12-yr climatology is too small to derive meaningful relationships.

TABLE OF CONTENTS

LIST OF FIGURES

ACKNOWLEDGEMENTS

First and foremost I would like to thank my advisor, Jim Steenburgh, for his invaluable meteorological knowledge, guidance, encouragement, and moral support throughout this process. I would also like to thank my committee members, John Horel and Andy Wood, for their enthusiasm and suggestions to this thesis.

Next, I would like to thank Neil Laird and the summer 2007 undergraduate students Benjamin Albright and Jessica Popp at Hobart and William Smith Colleges who performed the initial LEP identification.

I would also like to thank the Colorado Basin River Forecast Center staff who originally introduced me to the hydrology of the Great Salt Lake Basin and helped answered all of my hydrology-related questions, especially Andy Wood, Michelle, Schmidt, and Kevin Werner.

Thanks also to the other graduate students in my research group, Trevor Alcott, Jeff Massey, Jon Rutz, and John McMillen for their insight and ideas; to Dan Tyndall for his advice on data assimilation; to Larry Dunn and Randy Graham for their interest and suggestions to the thesis; to Steve Summy for his vast COOP station knowledge; to Randy Julander for his vast SNOTEL station knowledge; to Utah State University for their COOP station dataset; to the snow safety staff at Alta Ski Area for their hourly Alta-Collins dataset; and especially to Trevor Alcott for his Matlab and data processing expertise, thesis editing, and countless hours spent sifting through radar data.

Special thanks to all of my friends who made my time in Utah absolutely unforgettable, especially Carolyn Stwertka, Annie Neuman, Sandra Anderson, Courtney Chisholm, Jeff Massey, Morgan Farley-Chrust, and Adam Varble, and Trevor Alcott.

Last but not least, I would like to thank my family and boyfriend, Stephen Schepel, for their unconditional love and support in the pursuit of my dreams, and to my parents, David and Gail, for making the long trek out to Utah to see my thesis defense.

This thesis is based upon work supported by the National Science Foundation under Grant AGS-0938611: Orographic Influences on Lake-Effect Precipitation. Any opinions, findings, and conclusions or recommendations expressed in this material are those of the author and do not necessarily reflect the views of the National Science Foundation.

# CHAPTER 1

# INTRODUCTION

Lake-effect precipitation is a potentially important component of the water cycle near large inland bodies of water, including the Great Salt Lake (GSL) of northern Utah. As a terminal lake within a closed hydrologic basin, the GSL serves as a collector and integrator of climate variability and change (Lall and Mann 1995; Lall et al. 1996; Mohammed and Tarboton 2011). Imbalances between lake inflows, which are dominated by surface-water runoff (66%) and direct precipitation on the lake (31%), and outflows, which consist entirely of evaporation, cause changes in lake level, area, and composition (e.g. salinity) that affect mineral industries, shoreline and aquatic ecosystems, natural resource management, and transportation (Arnow 1980; Gwynn 1980; Mohammed and Tarboton 2011; USGS 2011).

Lake-effect precipitation (primarily in the form of snowstorms) occurs over northern Utah several times per year (Steenburgh et al. 2000; Alcott et al. 2012) and contributes to the GSL water budget through direct precipitation on the lake and the buildup of a mountain snowpack that drives much of the surface-water runoff within the GSL basin and serves as the primary water resource for 400,000 people in Salt Lake City (Salt Lake City Department of Public Utilities 1999). Lake-effect precipitation also provides a path for water recycling (Eltahir et al. 1996) since evaporation from the lake contributes to a portion of the water mass that falls as precipitation (Onton and

Steenburgh 2001) and eventually returns as surface-water runoff.

Great Salt Lake-effect (GSLE) precipitation periods can generate substantial rain and snow accumulations. Carpenter (1993) describes a GSLE snowstorm that produced up to 69 cm of snow in the Salt Lake Valley and 102 cm in the adjacent Wasatch Mountains (see Fig. 1.1 for geographic locations). In an analysis of the 22–27 Nov 2001 "hundred-inch storm," Steenburgh (2003) attributed 1.45 cm of the snow-water equivalent (SWE) that fell at Salt Lake City International Airport and 5.54 cm of the SWE that fell at the Alta-Collins observing site in the adjacent Wasatch Mountains to two lake-effect periods. Beyond potential impacts on water resources, GSLE helps fuel Utah's \$1.2 billion $yr^{-1}$ (U.S. dollars) ski industry and reputation for the "Greatest Snow on Earth" (Steenburgh and Alcott 2008; Gorrell 2011).

Climatological studies illustrate the general characteristics of GSLE, including its underlying environmental conditions, seasonality, and spatial distribution (Carpenter 1993; Steenburgh et al. 2000; Alcott et al. 2012). GSLE occurs during cold-air outbreaks when localized sensible and latent heating over the GSL leads to the development of precipitating moist convection (Carpenter 1993; Steenburgh et al. 2000; Steenburgh and Onton 2001). Alcott et al. (2012) identify an average of 13 GSLE periods per cool season (16 Sep – 15 May), with fall and spring peaks in period frequency separated by a mid-winter minimum. Radar reflectivity indicates that GSLE precipitation is greatest to the south and east of the GSL, and most common in the overnight and early morning hours when land-breeze convergence contributes to convective initiation (Steenburgh et al. 2000; Steenburgh and Onton 2001; Onton and Steenburgh 2001).

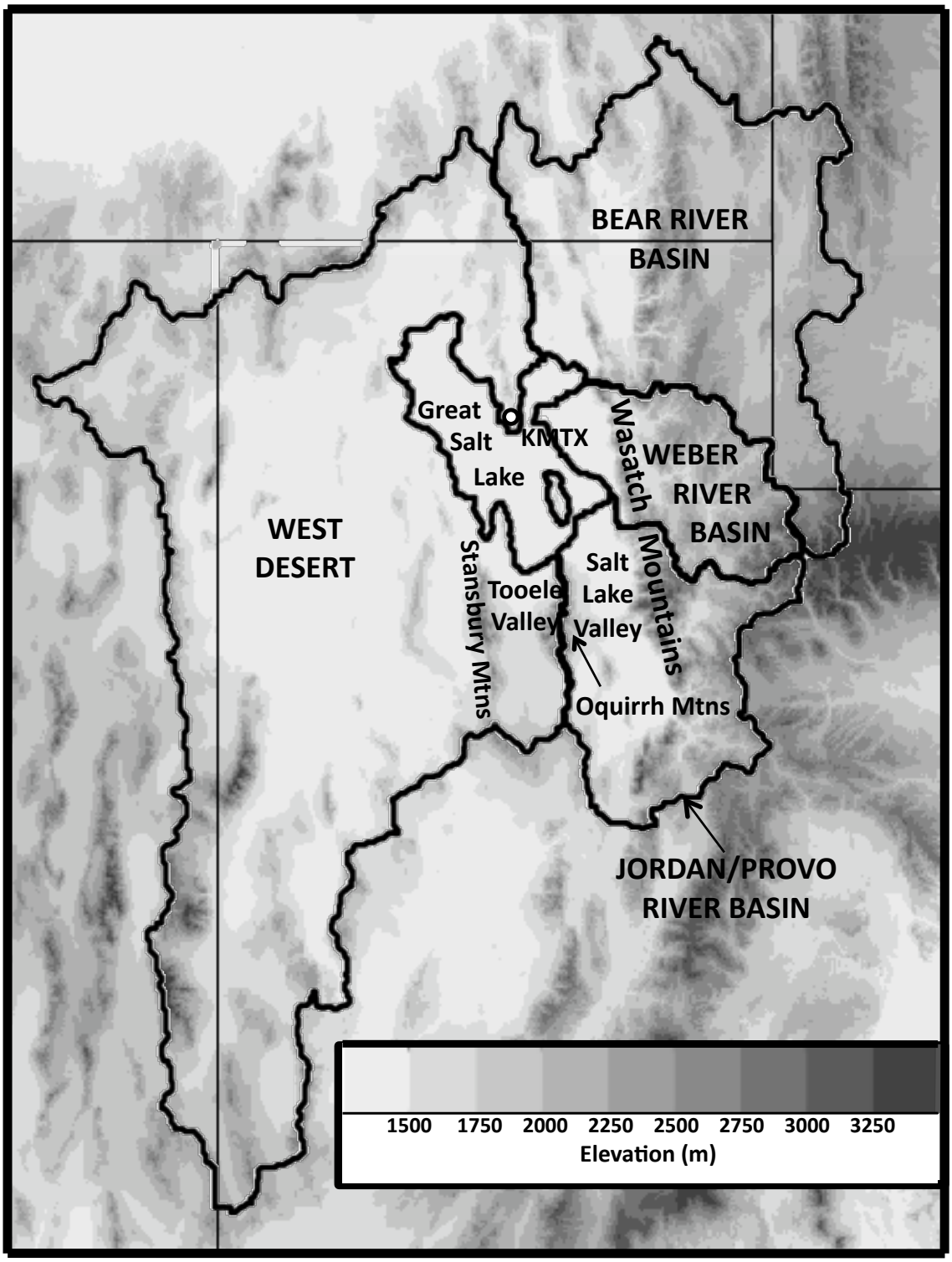


Figure 1.1. Map of GSL basin, sub-basins, and surrounding topography.

Despite progress in characterizing the climatology and dynamic of GSLE precipitation, no previous study has attempted to estimate *how much* precipitation is produced seasonally by GSLE. A better understanding of the seasonality of GSLE precipitation will help advance quantitative precipitation forecasting techniques during lake-effect periods and provide perspective for climate scientists in predicting how GSLE precipitation may vary in the future.

Quantitative estimates have been made for seasonal lake-effect snowfall near the Laurentian Great Lakes using a variety of approaches (e.g., Changnon 1968; Eichenlaub 1970; Braham and Dungey 1984; Scott and Huff 1996, 1997). For example, Changnon (1968) compares snowfall amounts near the climatological upwind (western) and downwind (eastern) shorelines of Lake Michigan, Eichenlaub (1970) examines how much snow is produced during periods when the synoptic conditions are favorable for lake effect, and Braham and Dungey (1984) and Scott and Huff (1996, 1997) calculate the enhancement relative to an estimate of non-lake-effect precipitation obtained by interpolating precipitation amounts from outside the lake-effect snowbelts. Scott and Huff (1996, 1997) examined the entire Great Lakes Basin and estimate that lake-effect more than doubles the mean wintertime snowfall east of Lake Superior, and yields increases of 90% southeast of Lake Huron, 35% east of Lake Michigan, and 40% east of Lakes Erie and Ontario.

Complex topography strongly influences precipitation around the GSL and precludes the application of relatively simple approaches like those used around the Laurentian Great Lakes. The GSL is oriented from northwest to southeast with the Wasatch Mountains to the east and the Oquirrh and Stansbury Mountains to the south

(Fig. 1.1). The lake has an average surface area of approximately 4400 $km^2$, making it much smaller than Lake Ontario (18960 $km^2$), the smallest of the Laurentian Great Lakes. The GSL basin spans four states: Utah, Wyoming, Nevada, and Idaho (Fig. 1.1) and encompasses a total area of 89000 $km^2$. Due to the small contribution of groundwater from the West Desert, however, the basin has an effective area of 55000 $km^2$ (Lall and Mann 1995; Johnson et al. 2004). Relatively little precipitation falls in the lower elevations and valley floors (10–65 cm annually), while much larger amounts occur in the mountains or higher elevations (100–130+ cm annually). Although orographically-forced precipitation gradients are common in mountainous regions, those of the GSL basin are comparatively large, and the associated ecosystem transitions are unique (Western Regional Climate Center 2011; Great Salt Lake Information System 2011).

In this research we develop and apply a technique to quantify the amount of precipitation produced during GSLE periods during the 1998–2009 cool-seasons (16 Sep – 15 May). As described in Chapter 2, the approach uses high-frequency radar-derived precipitation estimates to produce an hourly resolution precipitation dataset from gauge-based daily (24-h) precipitation observations. We then use this dataset to partition the observed precipitation into lake-effect and non-lake effect periods. We evaluate the technique in Chapter 3, and present results concerning the magnitude, spatial distribution, seasonality, and interannual variability of GSLE precipitation in Chapter 4. We discuss the implications of our findings and some of the limitations of the technique in the summary and conclusions that follow in Chapter 5.

# CHAPTER 2

# DATA AND METHODS

The developed method involves the generation of quantitative lake-effect period precipitation estimates and was applied to the 1998–2009 cool seasons (i.e., 16 Sep–15 May, with the year defined by the calendar year at the end of the cool season), which contained 128 lake-effect periods. Lake-effect periods are those identified in Alcott et al. (2012) and are based on visual inspection of KMTX WSR-88D radar reflectivity imagery. KMTX is at 2111 m AMSL (823 m above mean lake level) on Promontory Point, a mountain peninsula in the northern half of the GSL (Fig. 1.1). Following Laird et al. (2009), lake-effect periods are defined as having at least one hour where any or all of the following are identifiable in radar imagery: (1) coherent, quasi-stationary precipitation features with a distinct connection to the lake; (2) shallow precipitation features distinguishable from large, transitory synoptic features; (3) precipitation features with increasing depth and/or intensity in the downwind direction. Table 2.1 presents a complete list of lake-effect periods with beginning and end times.

Generation of hourly SWE records to enable quantification of lake-effect period precipitation (in snow water equivalent, hereafter *SWE*) follows the approach of Wüest et al. (2010) who used radar-based disaggregation of daily precipitation gauge observations to produce an hourly SWE dataset for Switzerland. Radar-base SWE estimates have a high temporal resolution (typically every 6–10 min), but suffer from low absolute

Table 2.1

Lake-effect period onset and ending times and evaluation stations

| Lake-Effect Period | Onset Time (UTC) | Ending Time (UTC) | Evaluation Stations |
|---|---|---|---|
| 1 | 23:36 11 Oct 1997 | 00:28 13 Oct 1997 | KSLC |
| 2 | 03:39 24 Oct 1997 | 20:41 24 Oct 1997 | KSLC |
| 3 | 02:19 24 Dec 1997 | 08:00 24 Dec 1997 | KSLC |
| 4 | 13:18 30 Jan 1998 | 05:03 31 Jan 1998 | KSLC |
| 5 | 22:40 11 Feb 1998 | 05:32 12 Feb 1998 | KSLC |
| 6* | 05:36 27 Feb 1998 | 20:32 27 Feb 1998 | |
| 7 | 04:26 04 Mar 1998 | 16:26 04 Mar 1998 | KSLC |
| 8 | 15:07 29 Mar 1998 | 17:21 29 Mar 1998 | KSLC |
| 9 | 03:25 30 Mar 1998 | 20:28 30 Mar 1998 | KSLC |
| 10 | 09:58 02 Apr 1998 | 19:56 02 Apr 1998 | KSLC |
| 11 | 05:04 07 Apr 1998 | 18:56 07 Apr 1998 | KSLC |
| 12 | 03:39 08 Apr 1998 | 16:53 08 Apr 1998 | KSLC |
| 13** | 03:56 15 Apr 1998 | 12:14 15 Apr 1998 | |
| 14 | 04:28 04 Oct 1998 | 14:21 04 Oct 1998 | KSLC |
| 15 | 13:18 16 Oct 1998 | 23:30 16 Oct 1998 | KSLC |
| 16 | 06:03 03 Nov 1998 | 18:15 03 Nov 1998 | KSLC |
| 17 | 04:03 06 Nov 1998 | 08:07 06 Nov 1998 | KSLC |
| 18 | 03:28 09 Nov 1998 | 10:09 10 Nov 1998 | KSLC |
| 19 | 13:09 19 Nov 1998 | 17:01 19 Nov 1998 | KSLC |
| 20 | 04:19 05 Dec 1998 | 23:00 05 Dec 1998 | KSLC, CLN |
| 21 | 19:59 06 Dec 1998 | 21:08 07 Dec 1998 | KSLC, CLN |
| 22 | 01:41 20 Dec 1998 | 08:22 20 Dec 1998 | KSLC |
| 23 | 10:55 20 Dec 1998 | 03:55 21 Dec 1998 | |
| 24 | 08:53 10 Feb 1999 | 09:20 11 Feb 1999 | KSLC, CLN |
| 25 | 11:14 05 Mar 1999 | 16:40 05 Mar 1999 | KSLC, CLN |
| 26 | 02:47 12 Mar 1999 | 12:44 12 Mar 1999 | KSLC, CLN |
| 27 | 06:10 02 Apr 1999 | 15:28 02 Apr 1999 | KSLC, CLN |
| 28 | 02:56 03 Apr 1999 | 11:39 03 Apr 1999 | KSLC, CLN |
| 29 | 03:23 04 Apr 1999 | 09:53 04 Apr 1999 | KSLC, CLN |
| 30 | 09:30 10 Apr 1999 | 15:03 10 Apr 1999 | KSLC |
| 31 | 05:40 05 May 1999 | 15:50 05 May 1999 | KSLC |
| 32 | 06:42 29 Oct 1999 | 16:23 29 Oct 1999 | KSLC |
| 33 | 16:20 21 Nov 1999 | 17:59 21 Nov 1999 | KSLC, CLN |
| 34 | 23:15 21 Nov 1999 | 22:46 23 Nov 1999 | KSLC, CLN |
| 35 | 04:59 03 Dec 1999 | 10:25 03 Dec 1999 | KSLC, CLN |
| 36 | 22:30 10 Dec 1999 | 13:28 11 Dec 1999 | KSLC, CLN |
| 37 | 02:10 14 Dec 1999 | 13:54 14 Dec 1999 | KSLC |
| 38 | 14:54 02 Jan 2000 | 21:36 02 Jan 2000 | KSLC, CLN |
| 39 | 10:37 03 Jan 2000 | 17:31 03 Jan 2000 | KSLC, CLN |
| 40 | 00:18 06 Jan 2000 | 10:24 06 Jan 2000 | KSLC, CLN |
| 41 | 11:47 10 Mar 2000 | 19:33 10 Mar 2000 | KSLC, CLN |
| 42* | 09:28 15 Apr 2000 | 14:25 15 Apr 2000 | |
| 43 | 06:47 19 Apr 2000 | 10:04 19 Apr 2000 | KSLC, CLN |

Table 2.1 continued

| Lake-Effect Period | Onset Time (UTC) | Ending Time (UTC) | Evaluation Stations |
|---|---|---|---|
| 44 | 09:39 24 Apr 2000 | 13:31 24 Apr 2000 | KSLC, CLN |
| 45 | 07:54 11 May 2000 | 15:58 11 May 2000 | KSLC |
| 46 | 09:05 12 May 2000 | 14:21 12 May 2000 | KSLC |
| 47* | 07:32 31 Oct 2000 | 14:14 31 Oct 2000 | |
| 48** | 14:20 01 Nov 2000 | 21:26 01 Nov 2000 | |
| 49** | 09:44 05 Nov 2000 | 18:57 05 Nov 2000 | |
| 50** | 17:22 06 Nov 2000 | 20:42 06 Nov 2000 | |
| 51 | 06:57 09 Nov 2000 | 20:23 09 Nov 2000 | KSLC |
| 52 | 10:00 10 Nov 2000 | 17:34 10 Nov 2000 | KSLC |
| 53 | 14:08 13 Nov 2000 | 22:29 13 Nov 2000 | KSLC, CLN |
| 54 | 23:32 15 Nov 2000 | 19:35 16 Nov 2000 | KSLC, CLN |
| 55 | 05:36 09 Apr 2001 | 16:15 09 Apr 2001 | KSLC, CLN |
| 56 | 06:38 22 Apr 2001 | 14:30 22 Apr 2001 | KSLC, CLN |
| 57 | 05:19 24 Oct 2001 | 08:11 24 Oct 2001 | KSLC |
| 58**° | 09:05 23 Nov 2001 | 04:41 24 Nov 2001 | |
| 59**° | 16:33 25 Nov 2001 | 16:35 27 Nov 2001 | |
| 60** | 07:36 28 Nov 2001 | 15:55 28 Nov 2001 | |
| 61 | 08:08 04 Dec 2001 | 17:20 04 Dec 2001 | KSLC, CLN |
| 62 | 10:59 11 Dec 2001 | 23:50 11 Dec 2001 | KSLC, CLN |
| 63 | 01:42 12 Dec 2001 | 16:32 12 Dec 2001 | KSLC, CLN |
| 64 | 14:36 15 Dec 2001 | 23:46 15 Dec 2001 | KSLC, CLN |
| 65 | 05:53 16 Jan 2002 | 17:51 16 Jan 2002 | KSLC |
| 66 | 15:18 18 Jan 2002 | 21:20 18 Jan 2002 | KSLC |
| 67 | 13:08 14 Mar 2002 | 17:26 14 Mar 2002 | KSLC, CLN |
| 68 | 07:37 15 Mar 2002 | 10:38 15 Mar 2002 | KSLC |
| 69 | 08:13 16 Apr 2002 | 13:03 16 Apr 2002 | KSLC, CLN |
| 70 | 09:13 29 Oct 2002 | 18:30 29 Oct 2002 | KSLC |
| 71 | 00:18 30 Oct 2002 | 06:52 30 Oct 2002 | KSLC, CLN |
| 72 | 11:21 11 Nov 2002 | 19:45 11 Nov 2002 | KSLC, CLN |
| 73 | 02:45 06 Apr 2003 | 04:36 06 Apr 2003 | KSLC, CLN |
| 74 | 05:05 07 Apr 2003 | 14:14 07 Apr 2003 | KSLC, CLN |
| 75* | 14:45 30 Oct 2003 | 01:18 31 Oct 2003 | |
| 76 | 04:31 01 Nov 2003 | 08:47 01 Nov 2003 | KSLC |
| 77 | 03:16 02 Nov 2003 | 18:18 02 Nov 2003 | |
| 78 | 15:05 22 Nov 2003 | 13:30 23 Nov 2003 | KSLC, CLN |
| 79 | 16:40 27 Dec 2003 | 01:45 28 Dec 2003 | KSLC, CLN |
| 80 | 20:05 03 Jan 2004 | 08:06 04 Jan 2004 | KSLC, CLN |
| 81 | 10:32 21 Apr 2004 | 16:38 21 Apr 2004 | KSLC, CLN |
| 82 | 11:35 29 Apr 2004 | 18:27 29 Apr 2004 | KSLC, CLN |
| 83* | 03:21 12 May 2004 | 14:22 12 May 2004 | |
| 84 | 07:11 13 May 2004 | 11:44 13 May 2004 | KSLC |
| 85 | 10:22 31 Oct 2004 | 07:10 01 Nov 2004 | KSLC |
| 86 | 12:41 20 Nov 2004 | 19:46 20 Nov 2004 | KSLC, CLN |
| 87 | 09:26 30 Mar 2005 | 21:58 30 Mar 2005 | KSLC, CLN |
| 88 | 02:10 27 Nov 2005 | 21:26 27 Nov 2005 | KSLC, CLN |

Table 2.1 continued

| Lake-Effect Period | Onset Time (UTC) | Ending Time (UTC) | Evaluation Stations |
|---|---|---|---|
| 89 | 06:03 14 Dec 2005 | 09:55 14 Dec 2005 | KSLC, CLN |
| 90 | 00:09 16 Jan 2006 | 20:44 16 Jan 2006 | CLN |
| 91 | 04:56 16 Feb 2006 | 21:46 16 Feb 2006 | KSLC, CLN |
| 92 | 10:18 12 Mar 2006 | 17:44 12 Mar 2006 | KSLC, CLN |
| 93 | 15:51 17 Apr 2006 | 17:58 18 Apr 2006 | KSLC, CLN |
| 94 | 16:30 20 Sep 2006 | 00:26 21 Sep 2006 | KSLC |
| 95 | 11:21 22 Sep 2006 | 21:00 22 Sep 2006 | KSLC, CLN |
| 96 | 16:11 17 Oct 2006 | 22:09 17 Oct 2006 | KSLC, CLN |
| 97 | 06:41 29 Nov 2006 | 19:08 29 Nov 2006 | CLN |
| 98 | 10:59 02 Dec 2006 | 19:44 02 Dec 2006 | KSLC, CLN |
| 99 | 10:42 05 Jan 2007 | 17:42 05 Jan 2007 | KSLC, CLN |
| 100 | 22:57 11 Jan 2007 | 03:17 12 Jan 2007 | CLN |
| 101 | 03:17 24 Feb 2007 | 15:52 24 Feb 2007 | KSLC, CLN |
| 102 | 01:57 30 Sep 2007 | 04:11 30 Sep 2007 | KSLC, CLN |
| 103 | 04:31 18 Oct 2007 | 11:25 18 Oct 2007 | CLN |
| 104 | 01:37 21 Oct 2007 | 13:40 21 Oct 2007 | KSLC, CLN |
| 105 | 01:10 21 Nov 2007 | 04:43 21 Nov 2007 | |
| 106 | 11:11 28 Nov 2007 | 17:10 28 Nov 2007 | KSLC, CLN |
| 107 | 02:12 02 Dec 2007 | 08:34 02 Dec 2007 | KSLC, CLN |
| 108 | 03:15 14 Dec 2007 | 04:02 15 Dec 2007 | CLN |
| 109 | 02:26 21 Dec 2007 | 23:33 21 Dec 2007 | KSLC, CLN |
| 110 | 07:03 27 Dec 2007 | 00:11 28 Dec 2007 | KSLC, CLN |
| 111 | 21:19 15 Jan 2008 | 19:47 16 Jan 2007 | CLN |
| 112 | 08:53 04 Feb 2008 | 05:45 05 Feb 2008 | KSLC, CLN |
| 113 | 05:02 26 Feb 2008 | 08:38 26 Feb 2008 | KSLC, CLN |
| 114 | 01:20 16 Mar 2008 | 18:05 16 Mar 2008 | KSLC, CLN |
| 115 | 14:54 29 Mar 2008 | 20:03 29 Mar 2008 | CLN |
| 116 | 03:26 10 Apr 2008 | 09:34 10 Apr 2008 | KSLC, CLN |
| 117 | 04:35 11 Apr 2008 | 18:01 11 Apr 2008 | KSLC, CLN |
| 118 | 09:55 16 Apr 2008 | 16:32 16 Apr 2008 | CLN |
| 119 | 06:00 20 Apr 2008 | 09:36 20 Apr 2008 | KSLC, CLN |
| 120 | 04:19 01 May 2008 | 16:25 01 May 2008 | KSLC, CLN |
| 121 | 21:06 11 Oct 2008 | 06:23 12 Oct 2008 | KSLC, CLN |
| 122 | 06:23 12 Oct 2008 | 13:40 13 Oct 2008 | KSLC, CLN |
| 123 | 05:53 05 Nov 2008 | 03:48 06 Nov 2008 | KSLC, CLN |
| 124 | 01:53 14 Dec 2008 | 12:10 14 Dec 2008 | KSLC, CLN |
| 125 | 03:11 26 Dec 2008 | 07:26 26 Dec 2008 | KSLC, CLN |
| 126 | 10:34 26 Dec 2008 | 09:28 27 Dec 2008 | KSLC, CLN |
| 127 | 14:09 27 Feb 2009 | 17:01 27 Feb 2009 | KSLC, CLN |
| 128 | 00:46 23 Mar 2009 | 07:11 24 Mar 2009 | KSLC, CLN |

*Missing level III radar data
**Missing level III and level II radar data
°Part of "hundred-inch" storm as described by Steenburgh (2003)

accuracy, especially in complex terrain (e.g., Westrick et al. 1999; Rasmussen et al. 2001). Daily precipitation gauge observations provide greater absolute accuracy, but lack sufficient temporal resolution to isolate the SWE produced during lake-effect periods, which are typically < 24-h in length. Therefore, we use the temporally resolved radar-based SWE estimates to disaggregate the precipitation gauge observations from a daily to hourly time resolution, preserving the daily SWE totals and enabling the separation of accumulated SWE into lake-effect and non-lake-effect periods. The method involves four steps: (1) construction of a serially complete precipitation gauge dataset, (2) calculation of radar-estimated hourly SWE rates, (3) disaggregation of precipitation gauge observations from a daily to hourly time resolution, and (4) accumulation of SWE amounts during lake-effect and non-lake-effect periods.

Construction of a serially complete precipitation gauge dataset

The serially complete precipitation gauge dataset uses daily SWE observations from National Weather Service COoperative Observer Program (COOP) and Natural Resources Conservation Service (NRCS) SNOwpack TELemetry (SNOTEL) stations (Fig 2.1). COOP and SNOTEL data were obtained from the Utah Climate Center at Utah State University and NRCS website, respectively. Most COOP stations are in valley locations and depend on citizen weather volunteers to provide manual SWE measurements at a 0.01 in (0.25 mm) resolution from a recording or non-recording 8-in-diameter (20.3 cm) precipitation gauge (NWS 1989; Daly et al. 2007). Most of the precipitation gauges are unshielded, with two exceptions in the study area (Salt Lake City International Airport, UT (KSLC) and Ogden Pioneer Power House, UT; NWS 1989; S. Summy, NWS, personal communication). Additionally, if the

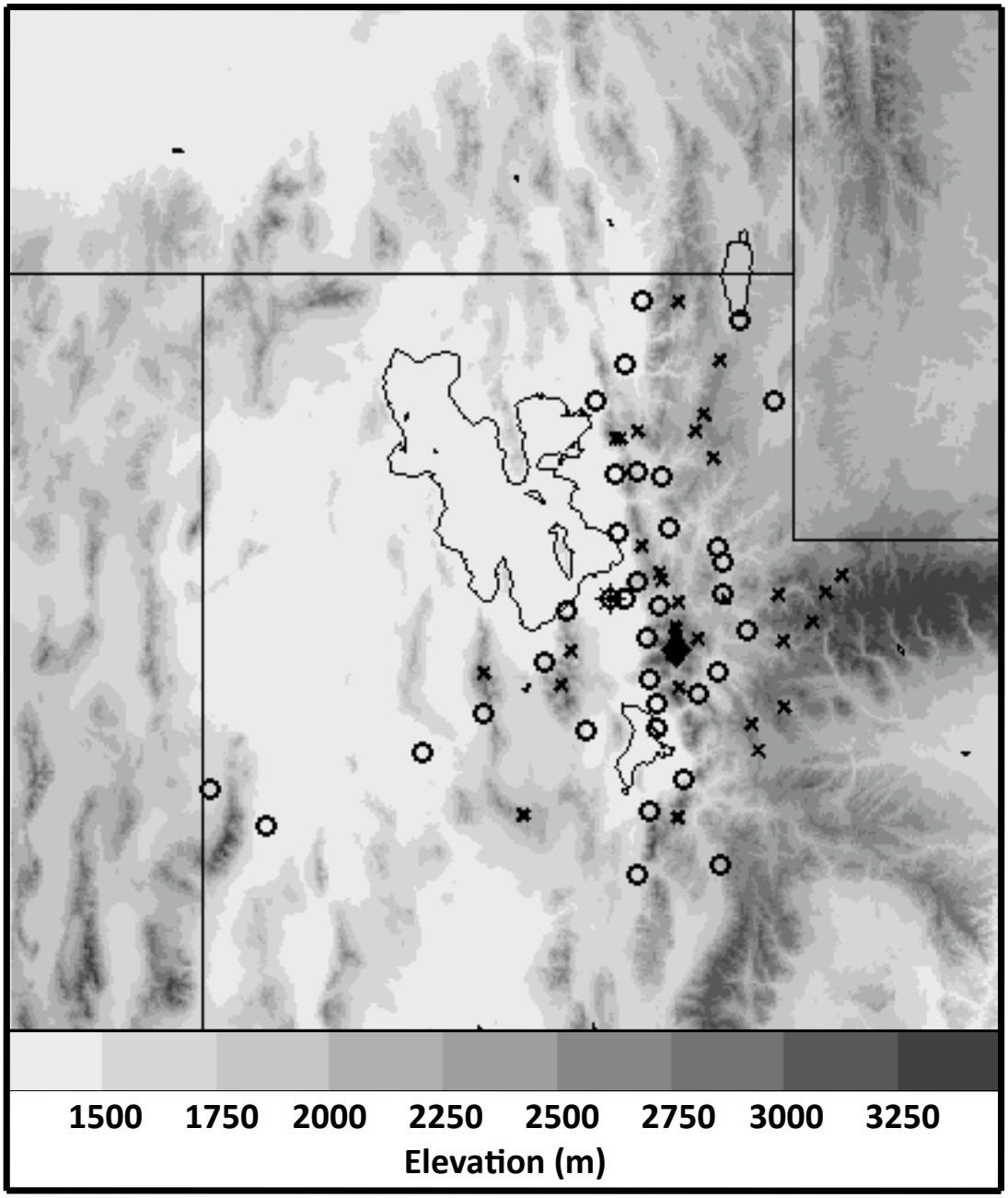


Figure 2.1. Map of surface stations used in the study. “o” indicates a COOP station. “x” indicates a SNOTEL station. “★” indicates Salt Lake City International Airport (KSLC). “◆” indicates Alta-Collins (CLN).

precipitation gauge measurement is questionable at KSLC, a manual measurement is taken and the observation record is adjusted accordingly (S. Summy, NWS, personal communication). Since the time of the observation is *not* consistent throughout the COOP network (varying from 1400–0700 UTC for the stations used in this study), it was obtained from the National Climatic Data Center (NCDC) to enable more accurate disaggregation of the daily SWE amounts.

SNOTEL stations are located primarily in the mountains and provide automated hourly and daily accumulated SWE measurements at 0.10 in (2.54 mm) resolution from a large storage precipitation gauge (Hart et al. 2005; NRCS 2011). The precipitation gauge is approximately 12 in (30.5 cm) in diameter, has an Alter shield around the orifice to reduce wind effects on catchment, and contains antifreeze to melt frozen precipitation and oil to prevent evaporation (Serreze et al. 1999; Wallis et al. 2007; R. Julander, NRCS, personal communication). This design makes the SNOTEL precipitation gauge more accurate for measuring frozen precipitation than a conventional tipping-bucket gauge, however, foreign objects falling into the gauge and thermal expansion and contraction of the liquid within the aluminum gauge can produce false precipitation fluctuations (Kuligowski 1997; R. Julander, NRCS, personal communication). The thermal expansion and contraction combined with low (2.54 mm) data resolution limits the accuracy of the hourly accumulations. Therefore, we opt to disaggregate the daily data.

Precipitation gauges provide a direct measurement at a discrete point, but are susceptible to systematic and random errors (Kuligowski 1997; Sieck 2007; Vasiloff et al. 2007). Systematic errors include undercatch during high winds, which likely averages

~10-15% for SNOTEL gauges (Rasmussen et al. 2011), and higher percentages for unshielded COOP gauges. Such errors are not accounted for in our statistics, but are discussed where relevant in the manuscript. SNOTEL observations are otherwise generally reliable, but mechanical issues and infrequent maintenance due to their remote location can result in errors and inconsistencies. COOP observations are subject to observer bias, which includes an underreporting of light events and overreporting of events divisible by five and ten-hundredths of an inch (Daly et al. 2007).

NRCS performs several levels of quality control on the daily SNOTEL observations, including manual inspection by a hydrologist, before archival on their website (NRCS 2011; R. Julander, NRCS, personal communication). Although this doesn't eliminate all sources of error, we assume the data is reliable and perform no additional quality control.

To help limit (but not eliminate) some of the problems with COOP observations, we only use COOP stations that report nearly continuously during the study period. Here, nearly continuously means missing less than 290 (~10%) of all possible daily SWE observations and less than 13 (~10%) of all possible daily SWE observations during lake-effect periods. This limits our analysis to the most frequently reporting COOP stations, which may reduce issues related to observer bias and identifies those stations that are likely the most reliable. We then examined all daily SWE amounts $\geq$ 50 mm and eliminated 5 that were clearly erroneous based on manual checks relative to surrounding observations.

For COOP stations meeting the criteria above, we used the normal ratio method (Paulhus and Kohler 1952; Young 1992; Eischeid et al. 2000) to estimate SWE on days

with missing or erroneous data. First, we calculate the climatological linear correlation coefficient between the observed daily SWE at the missing data station and surrounding COOP stations. This is done by month to account for seasonality in the spatial distribution of SWE. Then, we compute a weight, $W_i$ for each surrounding station *i,* from

$$W_i = \frac{r_i^2 (n_i - 2)}{1 - r_i^2}$$

where $r_i$ is the correlation coefficient between station *i* and the missing data station and $n_i$ is the number of days used to calculate the correlation coefficient (Eischeid et al. 2000; Young 1992). Finally, we calculate the SWE estimate, *M*, from

$$M = \sum_{i=1}^{n} w_i s_i$$

where $s_i$ is the SWE observation at station *i,* and $w_i$, the relative weight at surrounding station *i*, is

$$w_i = \frac{W_i}{\sum_{i=1}^{n} W_i}.$$

In calculating *M*, we use only the four most highly correlated surrounding stations (i.e., $n$=4) since Eischeid et al. (2000) found that the inclusion of more than four stations does not significantly improve the estimate, and in some cases may actually skew it. Further, due to the wide variation in COOP station observing times, only surrounding stations that report within 3-h of the missing-data station are used in the SWE estimate.

The SNOTEL station records are more complete than the COOP station records

with no more than 9 days of missing SWE observations at any station. Since SNOTEL stations report *accumulated* SWE, we assume no SWE fell on these missing days if there was no change in accumulated SWE between the preceding and following days. Otherwise we use an estimate based on the normal ratio above applied to surrounding SNOTEL stations.

Calculation of radar-estimated hourly SWE amounts

Estimating precipitation rate from radar reflectivity typically involves the use of an empirically derived power-law (i.e., *Z*–*R*) relationship of the form

$$Z = aR^b$$

where $Z$ is the radar reflectivity factor ($mm^6\ m^{-3}$), $R$ is the rainfall rate ($mm\ h^{-1}$), and $a$ and $b$ are constants (Doviak and Zrnic 1993; Rinehart 2004). The optimal *Z*–*R* relationship varies with storm type, precipitation type, and location (Rinehart 2004; Doviak and Zrnic 1993; Rasmussen et al. 2003). For estimating precipitation rates during snow, previous studies have derived an analogous *Z*–*S* (using S for SWE-rate during snow) relationship with $a$ ranging from 40–3300 and $b$ ranging from 0.88–2.2 (Gunn and Marshall 1958; Ohtake and Henmi 1970; Sekon and Srivastava 1970; Carlson and Marshall 1972; Puhakka 1975; Fujiyoshi 1990; Rasmussen 2003; WDTB 2011). For KMTX, Vasiloff (2001) recommends $Z = 75S^2$, which provides a nearly one-to-one linear fit between storm-total radar estimates and precipitation-gauge observations in the GSL basin, although considerable variability exists in the quality of fit from station to station. The National Weather Service (NWS) Warning Decision Training Branch presently recommends $Z = 40S^2$ for snowstorms in the Intermountain West. We have

used the Vasiloff (2001) relationship, although both relationships yield the same results since the disaggregation process is sensitive only to the exponent *b*, not the coefficient *a*.

Reflectivity values come from the lowest elevation scan (~0.5°) of the KMTX radar. For each scan, the maximum radar reflectivity in a nine-pixel stencil (i.e. a 3x3 grid of local pixels) centered on each COOP and SNOTEL station is identified and converted to a SWE rate. The nine-pixel stencil helps minimize the effects of wind displacement of the snow from the elevated radar level to ground-level observing site (Doviak and Zrnic 1993). SWE rates are converted into SWE amounts over each *interval,* defined as the time between radar scans, by taking the average SWE rate of the surrounding radar scans and multiplying it by the interval. Hourly SWE amounts are based on the summation of the SWE amounts calculated for all intervals during a given hour. This process is completed for all hours during all observing periods with lake-effect SWE.

To minimize storage space and processing time, we primarily use radar data archived in level III [a.k.a. NEXRAD Information Dissemination Service (NIDS)] format (Baer 1991), which has a reflectivity resolution of 5 dBZ and a spatial resolution of 1º x 1 km. The level III data is typically available every 6–10 min, but there are reporting gaps. SWE amounts during radar outages of 3-h or less are estimated in the same manner as above, by taking the average SWE rate of the scans surrounding the outage and multiplying it by the length of the outage. For lake-effect periods with radar outages greater than 3-h (9.4% of all lake-effect periods, Table 2.1), hourly SWE amounts are estimated using level II data, which has the same spatial resolution (1° x 1 km) as level III, but a much higher data resolution (0.5 dBZ; Crum et al. 1993). If level II radar data

are also missing (5.5% of all lake-effect periods, Table 2.1) hourly SWE amounts are estimated by interpolating 3-h SWE rates from the North American Regional Reanalysis (NARR), which has a 32 km spatial resolution (Mesinger et al. 2006).

Disaggregation of daily precipitation gauge observations

Using the hourly radar-estimated SWE, the disaggregated hourly precipitation gauge SWE accumulation, $G_t$, is calculated from:

$$G_t = \frac{E_t}{\sum_{t=1}^{24} E_t} G_d$$

where $E(t)$ is the radar-derived hourly SWE estimate, $G_d$ is the daily precipitation gauge observation, and $t$ is the hour (Wüest et al. 2010). This disaggregation is performed during all observation times that correspond to lake-effect periods.

The disaggregation significantly reduces quantitative biases produced by radar-derived SWE estimates, but does not completely eliminate them (Wüest et al. 2010; Doviak and Zrnic 1993; Vasiloff 2001; Rasmussen et al. 2003). In areas with complete radar beam blockage, the disaggregation will completely smooth the daily precipitation gauge total over all 24 hours (i.e. the same SWE amount will be recorded for each hour). For this reason, stations lying in areas with complete radar beam blockage were eliminated from the analysis (Fig. 2.2).

Accumulation of SWE amounts

The disaggregated hourly SWE amounts are then partitioned into lake-effect and non-lake-effect periods based on the onset and ending times defined for each lake-effect

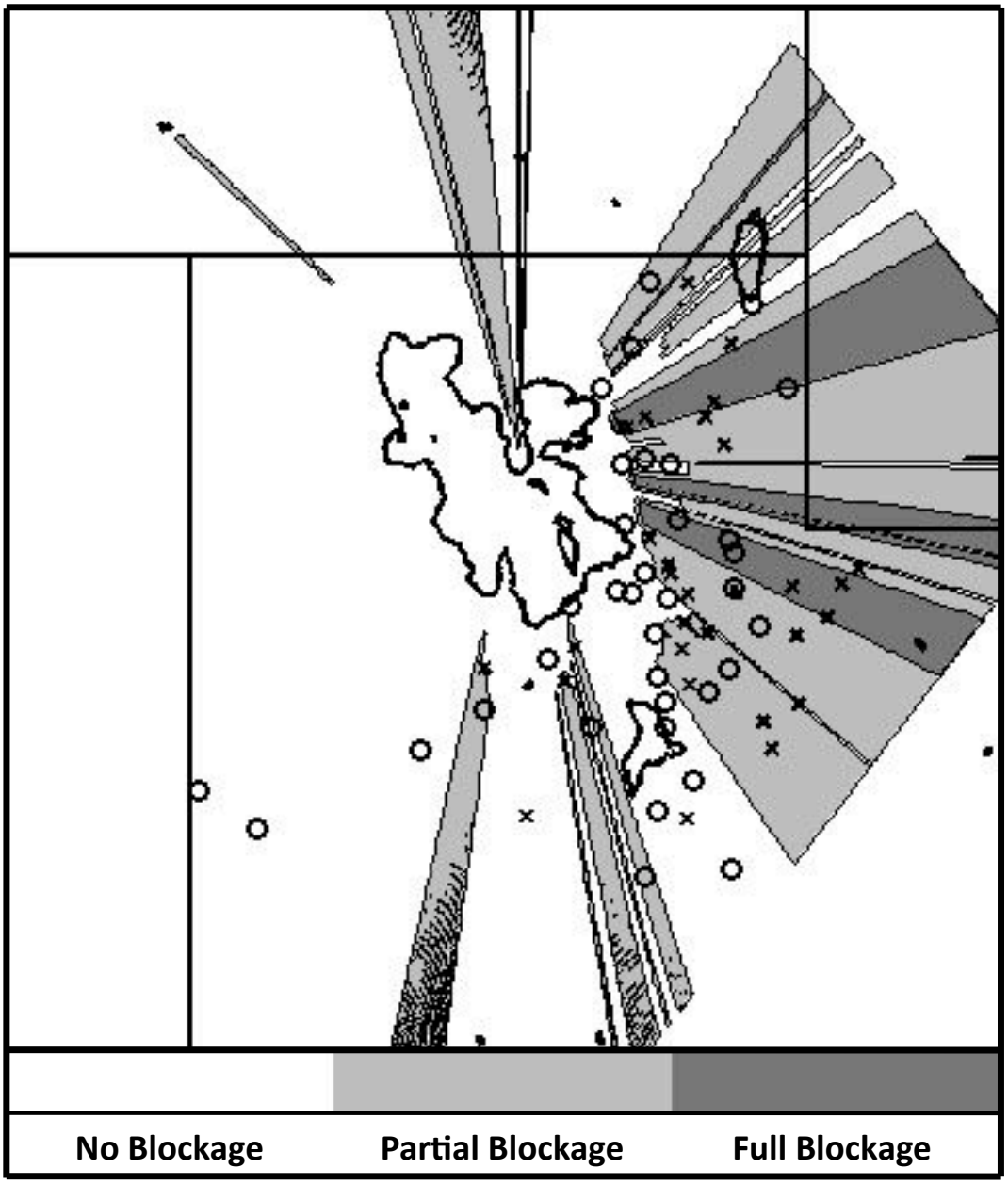


Figure 2.2. Map of radar beam blockage and surface stations used in the study. "o" indicates a COOP station. "x" indicates a SNOTEL station.

period (Table 2.1.). Since it is not possible to separate the dynamical, lake-effect, and orographic processes contributing to SWE during lake-effect periods, the SWE quantified in this study is not produced solely by the influence of the GSL. Therefore, we refer to it as lake-effect period SWE, and discuss this issue later in the thesis.

# CHAPTER 3

## EVALUATION OF APPROACH

To evaluate the accuracy of the disaggregation method, we compare disaggregated estimates of hourly and total SWE during lake-effect periods with reliable hourly gauge-based observations at two surface stations: Salt Lake City International Airport (KSLC) and Alta-Collins (CLN). The disaggregated estimates derive from daily (0000–0000 UTC) SWE accumulations summed from the hourly observations. This enables a direct evaluation that is not possible at sites with only daily data.

KSLC is a manually augmented Automated Surface Observing System (ASOS) station operated by the Salt Lake City NWS Weather Forecasting Office within the Salt Lake Valley at an elevation of 1288 m (Fig. 2.1). During the first part of the study period, the station was equipped with a heated tipping bucket, which was replaced with an All-Weather Precipitation Accumulation Gauge (AWPAG) in Jul 2004 (Groisman et al. 1999; Greeney et al. 2007; NOAA, NWS 2011). The heated tipping bucket measures hourly SWE at a resolution of 0.010 in (0.25 mm) and works by melting frozen precipitation before it enters the tipping apparatus (Groisman et al. 1999). The AWPAG weighs accumulated SWE at a resolution of 0.010 in (0.25 mm) and is accompanied by a wind shield to reduce undercatch (Greeney et al. 2007; Tokay et al. 2010). KSLC data was obtained from NCDC.

CLN is a mid-mountain (2945 m) site in Little Cottonwood Canyon (Fig. 2.1) run

by the snow-safety staff at Alta Ski Area. Hourly SWE is measured at a resolution of 0.010 in (0.25 mm) using a shielded 8-in weighing gauge. Like SNOTEL gauges, the CLN gauge contains antifreeze to minimize freezing of the accumulated snow and water mixture. The snow safety staff at Alta Ski Area collected and provided the CLN data.

The hourly SWE observations from KSLC and CLN were not subjected to quality control. We concentrate the evaluation on lake-effect periods that coincide with days with complete hourly data coverage at each station (Table 2.1). The coverage at KSLC is largely complete, but at CLN, lake-effect periods are mainly confined to Nov–Apr when the ski area is in operation. Additionally, the 1998–1999 seasons are not included in the CLN evaluation due to incomplete data.

We evaluate the accuracy of the disaggregation technique using scatter plots, frequency distributions, and three metrics: the mean bias error, mean absolute error, and total percent error. The mean bias error is

$$\frac{1}{n}\sum E - O$$

where $E$ is the disaggregated estimate, $O$ is the observed value, and $n$ is the number of data pairs. The mean absolute error does not take into account the sign of the error and follows

$$\frac{1}{n}\sum |E - O|.$$

Finally, the total percent error is evaluated from

$$\frac{\sum E - O}{\sum O}.$$

Figure 3.1a shows a scatter plot of disaggregated vs. observed SWE at KSLC during lake-effect hours. There are 1199 hourly estimates with a correlation of 0.75. The large amount of scatter shows the hourly estimates have some errors that appear to be randomly distributed. Figure 3.2a shows lake-effect period totals for KSLC. When the disaggregated hourly estimates are integrated over a longer time period (i.e. over an entire lake-effect period), they have a much higher correlation (0.92) to observed amounts.

The mean absolute and bias errors for disaggregated period-total SWE are 0.46 mm and -0.02 mm, respectively. The small bias error is reflected in the bias-error frequency distribution, which is quasi-normal with limited skew (Fig.3.3a). The quasi-normal distribution of bias error shows that the hourly positive and negative errors are quasi-random and largely cancel when integrated over longer time periods.

The scatter plot of disaggregated vs. observed SWE at CLN during lake-effect hours exhibits similar scatter and a slightly larger correlation of 0.76 (Fig. 3.1b). Like KSLC, the errors appear to be randomly distributed, and when integrated for lake-effect periods are nearly linear (0.99 correlation; Fig. 3.2b).

The mean absolute and bias errors for disaggregated period-total SWE at CLN are 1.21 mm and -0.95 mm, respectively. The bias error frequency distribution is quasi-normal with a larger negative skew than KSLC (Fig. 3.3b). The positive errors do not quite cancel the negative errors, revealing the tendency of the method to underestimate SWE during lake-effect periods at CLN.

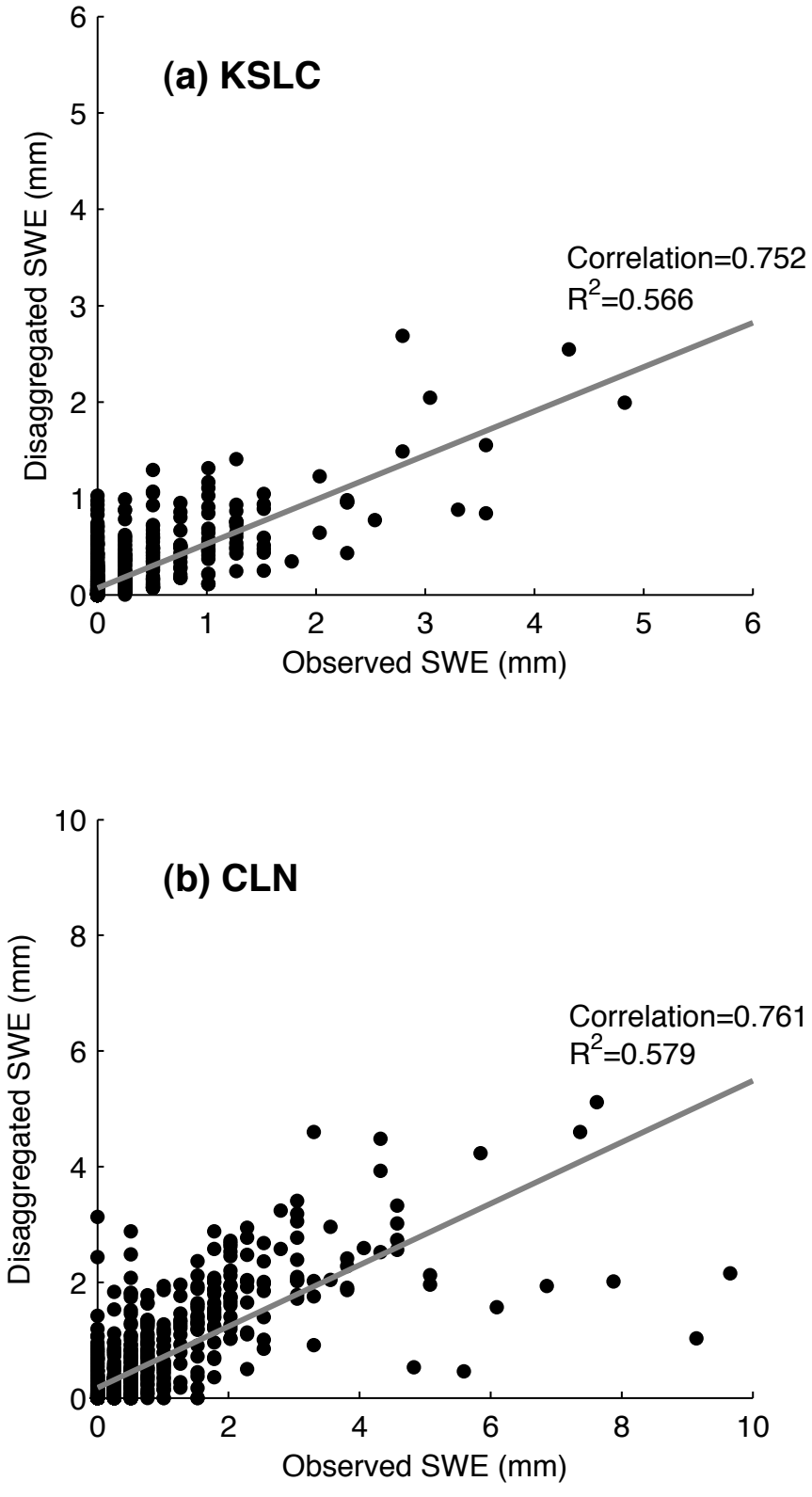


Figure 3.1. Hourly disaggregated SWE vs. observed SWE for (a) KSLC and (b) CLN.

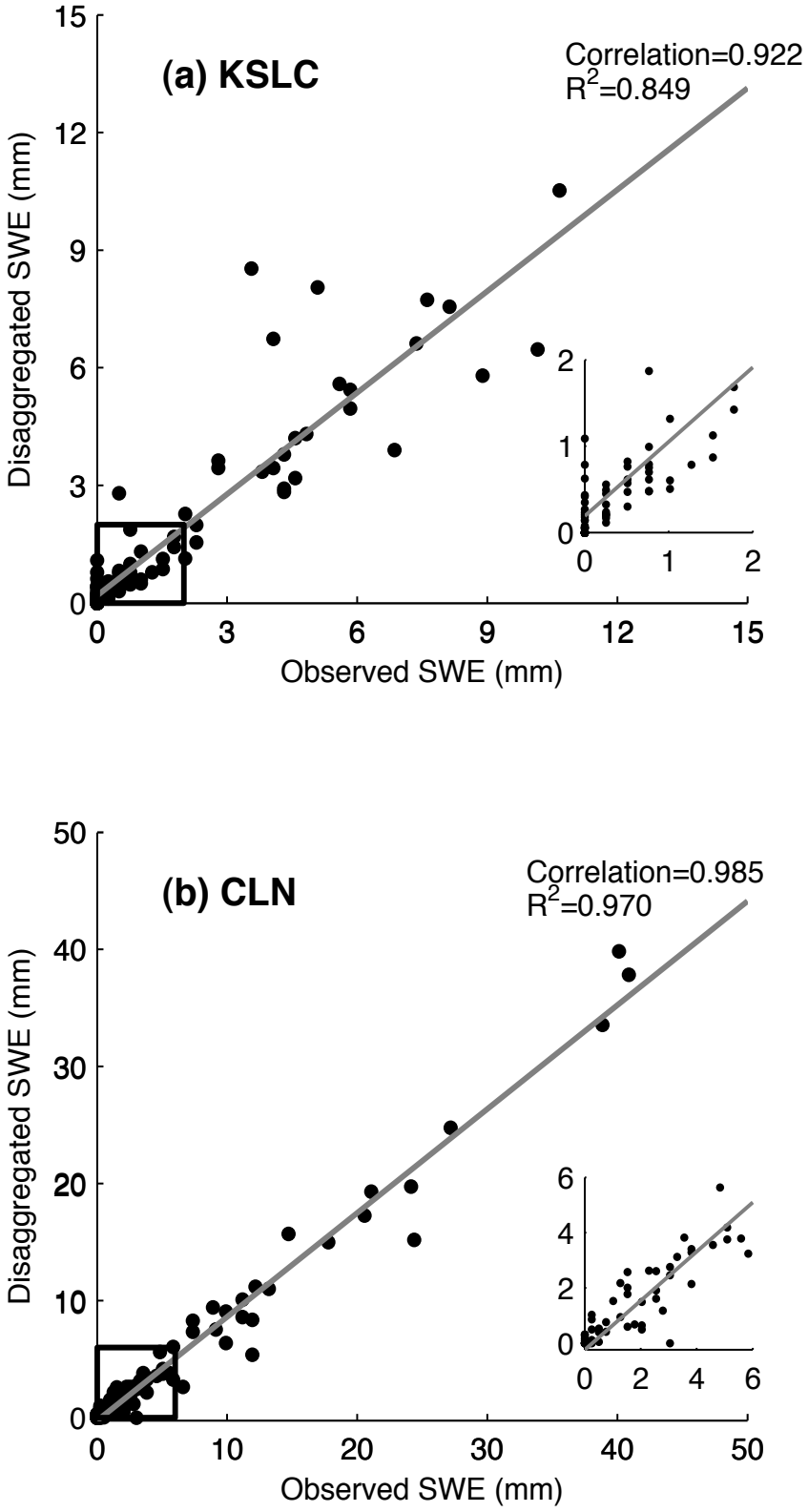


Figure 3.2. Lake-effect period total disaggregated SWE vs. observed SWE for (a) KSLC and (b) CLN.

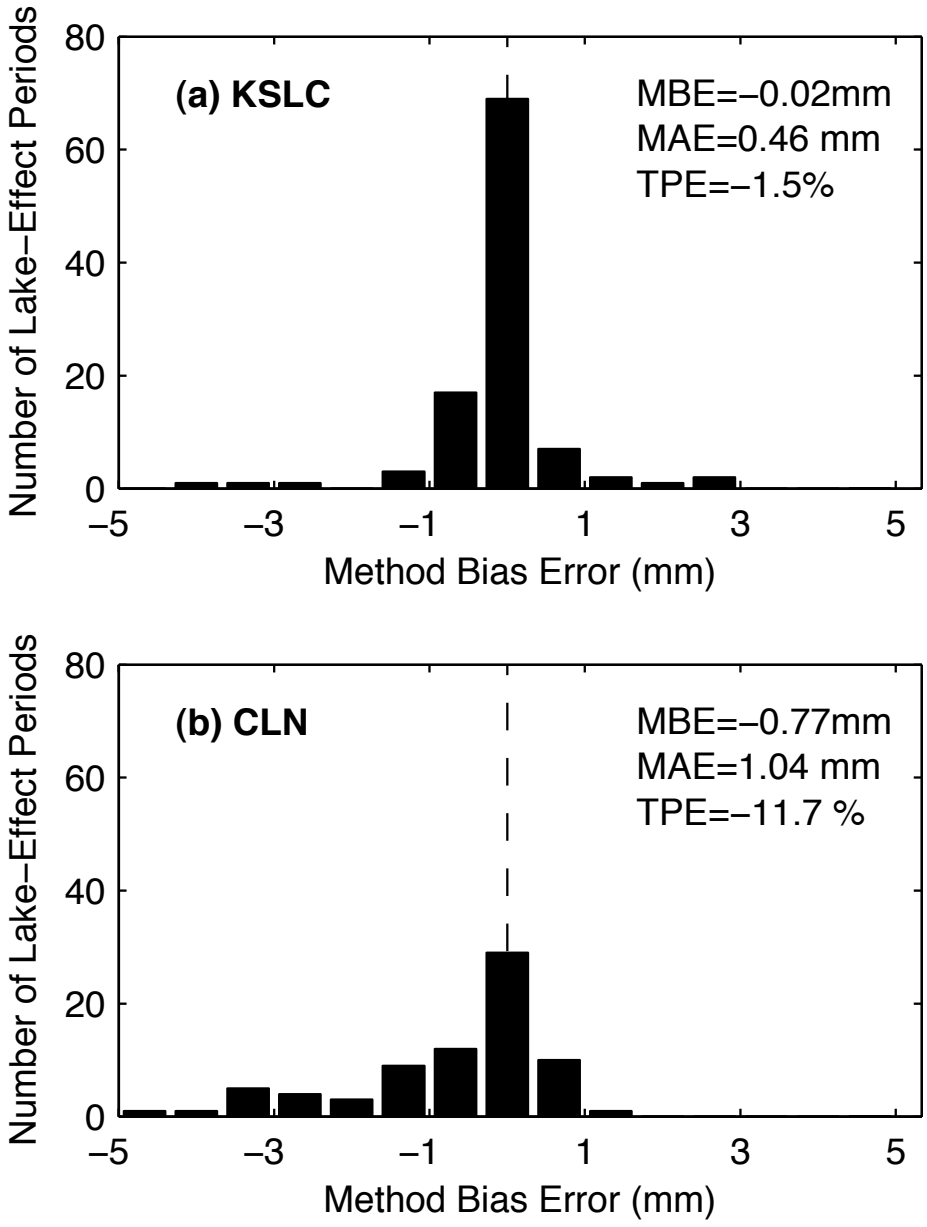


Figure 3.3. Frequency distribution of method error by lake-effect period for (a) KSLC and (b) CLN. CLN has two outlying errors of -6.56 mm and -9.21 mm (not shown). Abbreviations include MBE for Mean Bias Error, MAE for Mean Absolute Error, and TPE for Total Percent Error.

Hourly disaggregation errors stem from several sources. The first is representativeness error arising from the volume (1° x 1 km) and point measurements made by the radar and precipitation gauge, respectively. In some instances, the radar estimated SWE might not be representative of the SWE that occurred at the collocated point location (e.g., Kitchen 1992; Habib et al. 2004).

The second is the use of a single Z–S relationship. One Z–S relationship cannot accurately represent actual SWE rates given the wide variety of water and ice particles during storms (Doviak and Zrnic 1993; Rasmussen 2001). Also contributing to Z–S errors at KSLC and/or CLN are issues related to the overshooting of shallow storms, evaporation and sublimation below the lowest-elevation radar scans, incomplete beam filling, and bright banding (Doviak and Zrnic 1993; Vasiloff 2001; Rasmussen 2003; Wüest et al 2010). If the radar overshoots a storm for a portion of the day, the disaggregation will underestimate the SWE rate during that period and overestimate it during the remainder of the day (Wüest et al. 2010). Likewise, if the precipitation seen by the radar evaporates or sublimates before reaching the gauge, the disaggregation will overestimate the SWE rate during that period. Both of these types of errors are common at valley sites like KSLC because the average height of the center of the lowest tilt radar scan from the KMTX radar is approximately 1500 m above the valley floor (Fig. 3.4a). When the radar beam intersects a melting layer it causes high reflectivity returns, resulting in false SWE intensity peaks in the disaggregation (Doviak and Zrnic 1993; Wüest et al. 2010). Incomplete beam filling can result in an underestimation of SWE in the disaggregation as the radar is only partially sampling the storm (Fig. 3.4b).

These quantitative errors appear to largely cancel when integrating over long

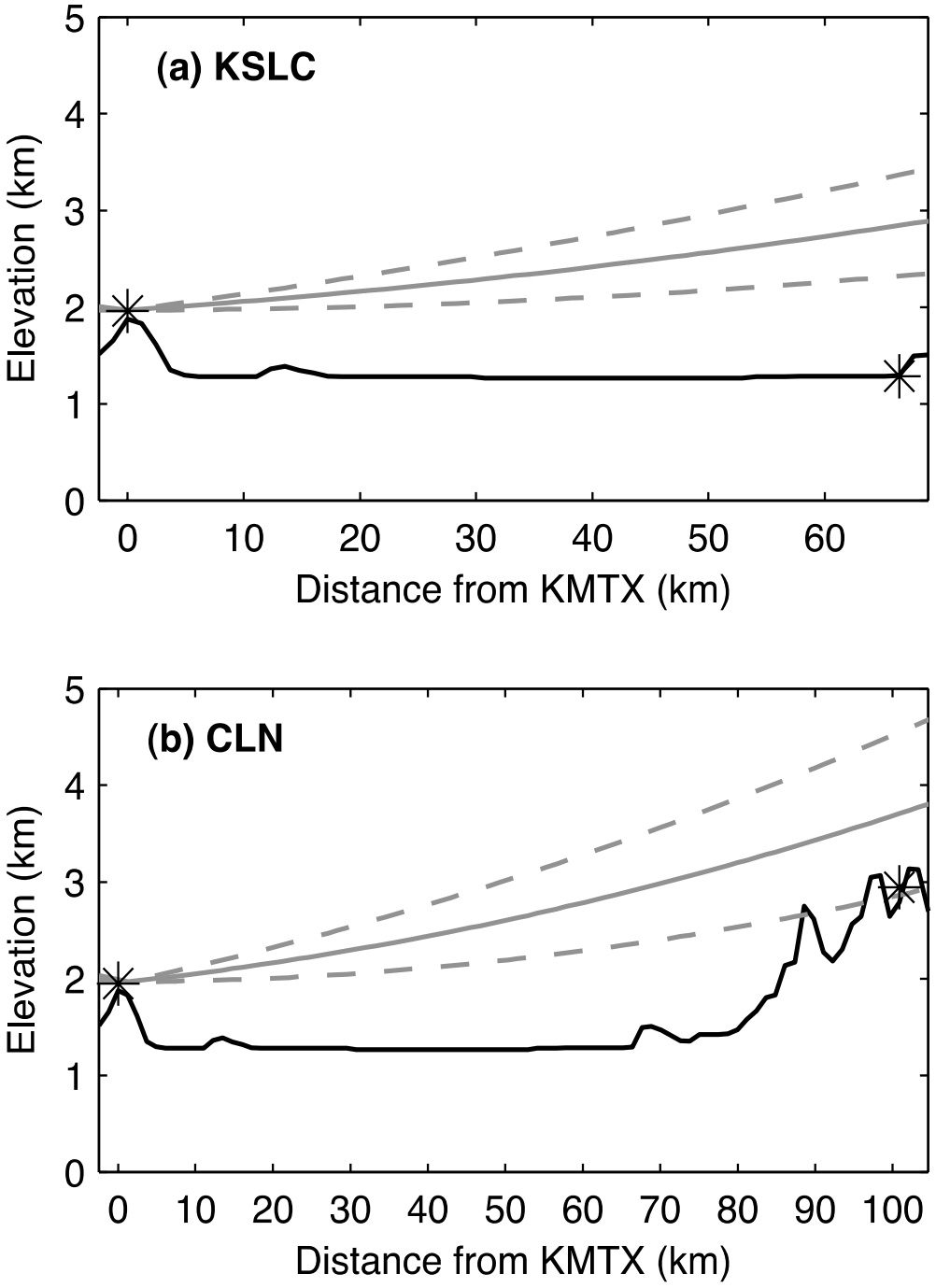


Figure 3.4. Cross section of the lowest elevation radar scan (0.5°) at KMTX for (a) KSLC and (b) CLN. The radar beam appears curved because its elevation is calculated relative to the earth's surface.

periods of time, resulting in a small total percent error of -1.5% and -14.8% at KSLC and CLN, respectively. Thus, we conclude that the method works reliably for estimating climatological lake-effect period SWE totals.

# CHAPTER 4

# RESULTS

## Cool-season mean and variability

To provide spatial context for the results for individual stations, Fig. 4.1 shows the frequency of occurrence of radar reflectivities greater than or equal to 10 dBZ during the 128 lake-effect periods identified for the climatology. 10 dBZ represents an approximate threshold of accumulating snow (Steenburgh et al. 2000). Neglecting the large frequencies of occurrence due to returns from vehicle traffic along major highways (Interstates 15, 80, and 215), the frequencies of occurrence are greatest to the south and east of the GSL, indicating that these areas should receive more SWE during lake-effect periods. Curiously, frequencies of occurrence are also large southeast of Utah Lake and the Bear River Range to the north. The large values in these areas are likely not associated with GSLE, but rather with other types of storms, including orographic and infrequent Utah lake-effect, that can occur in concert with GSLE. Thus, it is important to note that the SWE amounts estimated in this study do *not* represent SWE produced solely by the influence of the GSL. Instead, they represent the SWE produced during periods when GSLE can be subjectively identified in radar imagery.

Similarly, the mean cool-season SWE produced during lake-effect periods (hereafter the *lake-effect period SWE*) is greatest at stations to the south and east of the GSL (Fig. 4.2). Upper-elevation sites in the Oquirrh Mountains and Wasatch Mountains

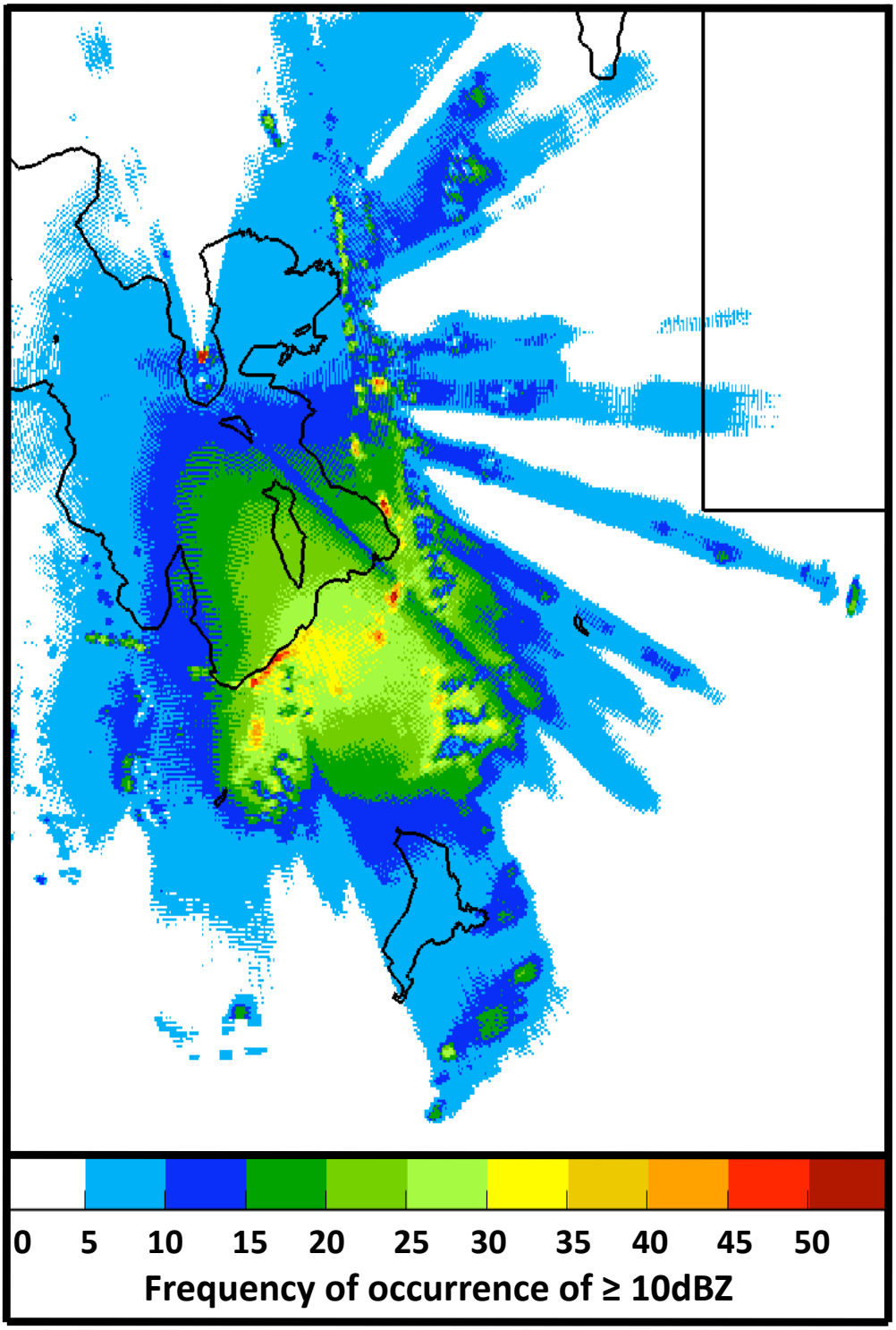


Figure 4.1. Frequency of occurrence of radar reflectivity ≥ 10 dBZ (%) during all lake-effect periods identified in climatology.

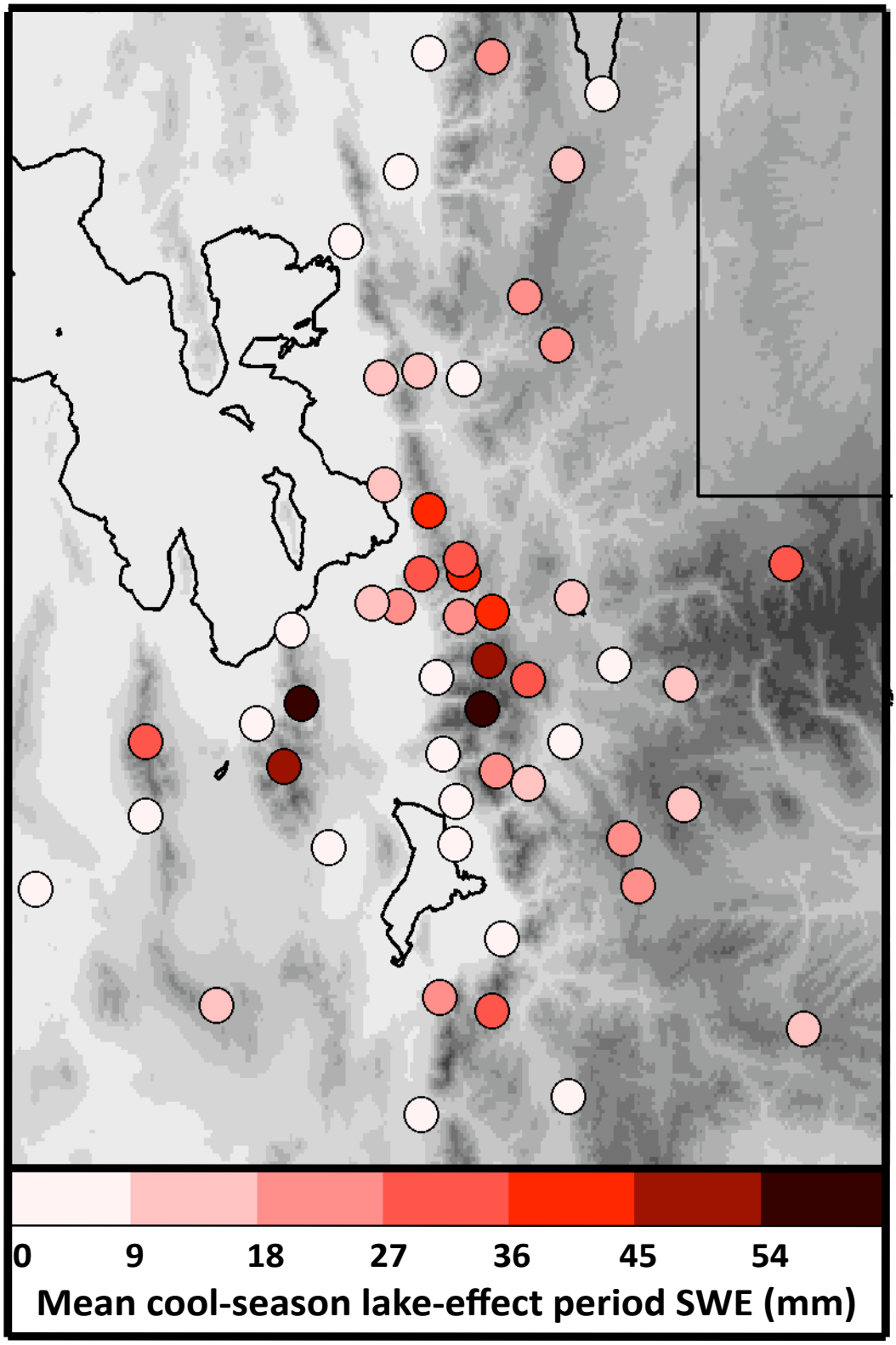


Figure 4.2. Mean cool-season lake-effect period SWE (mm) for stations in the GSL basin. Maximum is 60.4 mm.

record the largest lake-effect period SWEs. Relatively large lake-effect period SWEs also occur in the Wasatch Mountains southeast of Utah Lake and the Bear River Mountains, corresponding to the areas with high frequencies of occurrence of greater than or equal to 10 dbZ that are outside of the influence of the GSL. Interestingly, many COOP stations in the Salt Lake and Tooele Valleys south and east of the GSL tend to observe less lake-effect period SWE than the SNOTEL stations. This discrepancy is due to both the location of the stations (COOP stations are located at much lower elevations and typically receive less SWE) and the measuring methods of the COOP observers. Most COOP precipitation gauges are unshielded, making undercatch a probable issue in COOP SWE observations.

Dividing the mean cool-season lake-effect period SWE by the total mean cool-season SWE yields the fraction of mean cool-season SWE produced during lake-effect periods (hereafter the *lake-effect period fraction*). This calculation removes the inherent SWE gradient from low amounts at valley sites to higher amounts at mountain sites and provides a more spatially coherent map of the fractional lake-effect period contribution to total cool-season SWE.

The largest lake-effect period fractions occur at stations south and east of the GSL, including those in the Oquirrh Mountains, Salt Lake Valley, and adjacent Wasatch Mountains (Fig. 4.3). Larger fractions also occur at the previously mentioned locations in the Bear River Mountains and southeast of Utah Lake. Fractions do not exceed 8.4%.

A strong contrast exists between COOP and SNOTEL lake-effect period fractions, demonstrating the possible undercatch issues of COOP precipitation gauges. Figure 4.4 shows the frequency distribution of lake-effect period fraction for COOP and

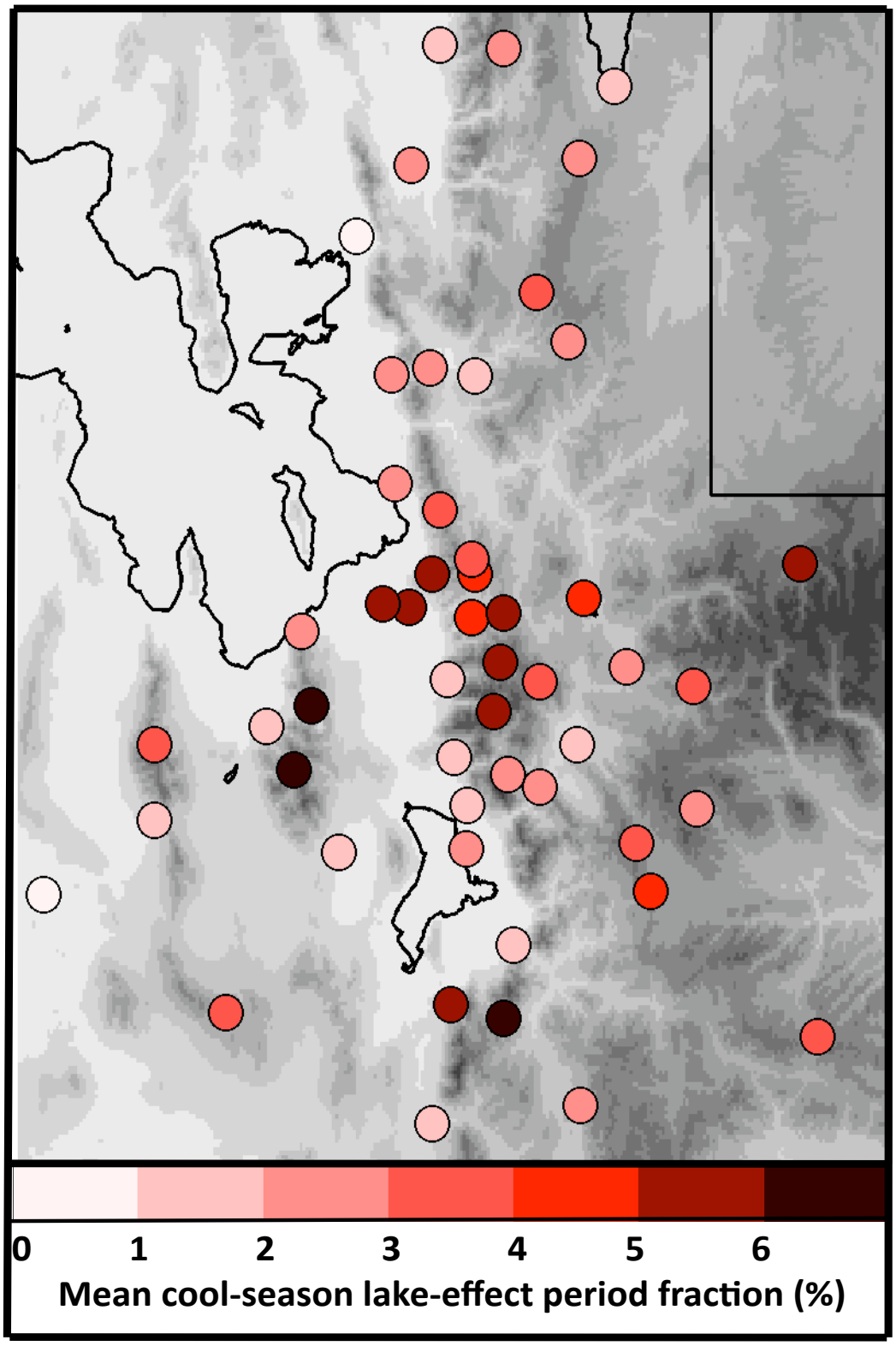


Figure 4.3. Mean cool-season lake-effect period fraction (%) for stations in the GSL basin. Maximum is 8.4%.

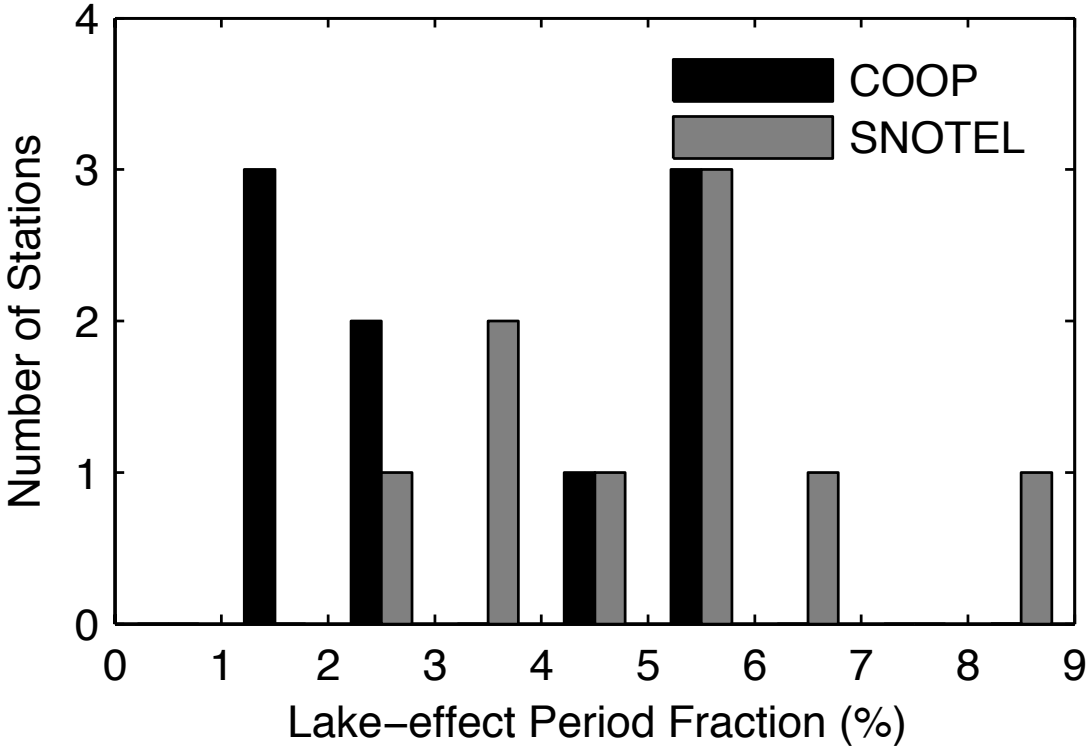


Figure 4.4. Frequency distribution of lake-effect period fraction by COOP and SNOTEL station. Black and grey dashed lines indicate mean COOP and SNOTEL lake-effect fractions, respectively from the stations show in Fig. 4.5.

SNOTEL stations south and east of the GSL (Fig. 4.5). Lake-effect period fractions average to 3.4% at COOP stations and 5.0% at SNOTEL stations. Although this could be the result of orographic processes during lake-effect periods, we hypothesize that it is also a partial result of gauge and reporting biases. In particular, there are three COOP stations at which the lake-effect period fraction is < 1.5%, despite the fact that all of these stations are located in the region where the frequency of occurrence of radar reflectivities greater than or equal to 10 dBZ is highest (Fig. 4.1). Furthermore, KSLC, which features a shielded precipitation gauge and manually augmented observations, has the highest lake-effect period fraction (5.78%) of the COOP stations.

SWE during lake-effect periods varies greatly from year to year, as illustrated by data from two sites located in the lake-effect period SWE maximum southeast of the GSL, KSLC and Snowbird (SBDU1). KSLC, which is located at lower altitudes in the Salt Lake Valley, has a mean cool-season lake-effect period fraction of 5.8%, but a range of 2.9–14.5% (Fig. 4.6a). Lake-effect period SWE averages 16 mm, with a range of 3.9–36.6 mm. SBDU1 has similar lake-effect period fractions (mean of 5.1%, range of 1.4–11.6%; Fig. 4.6b), but larger amounts (mean of 60.4 mm, range of 13.6–127.4 mm), which reflects its higher altitude location.

Both sites exhibit a prominent peak in lake-effect period SWE and fraction during the 2001–2002 cool-season when two intense lake-effect periods occurred during the so-called “hundred-inch storm” of late Nov 2001 (Steenburgh 2003). The latter of the two lake-effect periods produced 20.8 mm of SWE at KSLC and 81.1 mm of SWE at SBDU1, nearly doubling the next largest amount of SWE to ever fall during a single lake-effect period (Fig. 4.7a-b). Removing the SWE that fell during the lake-effect

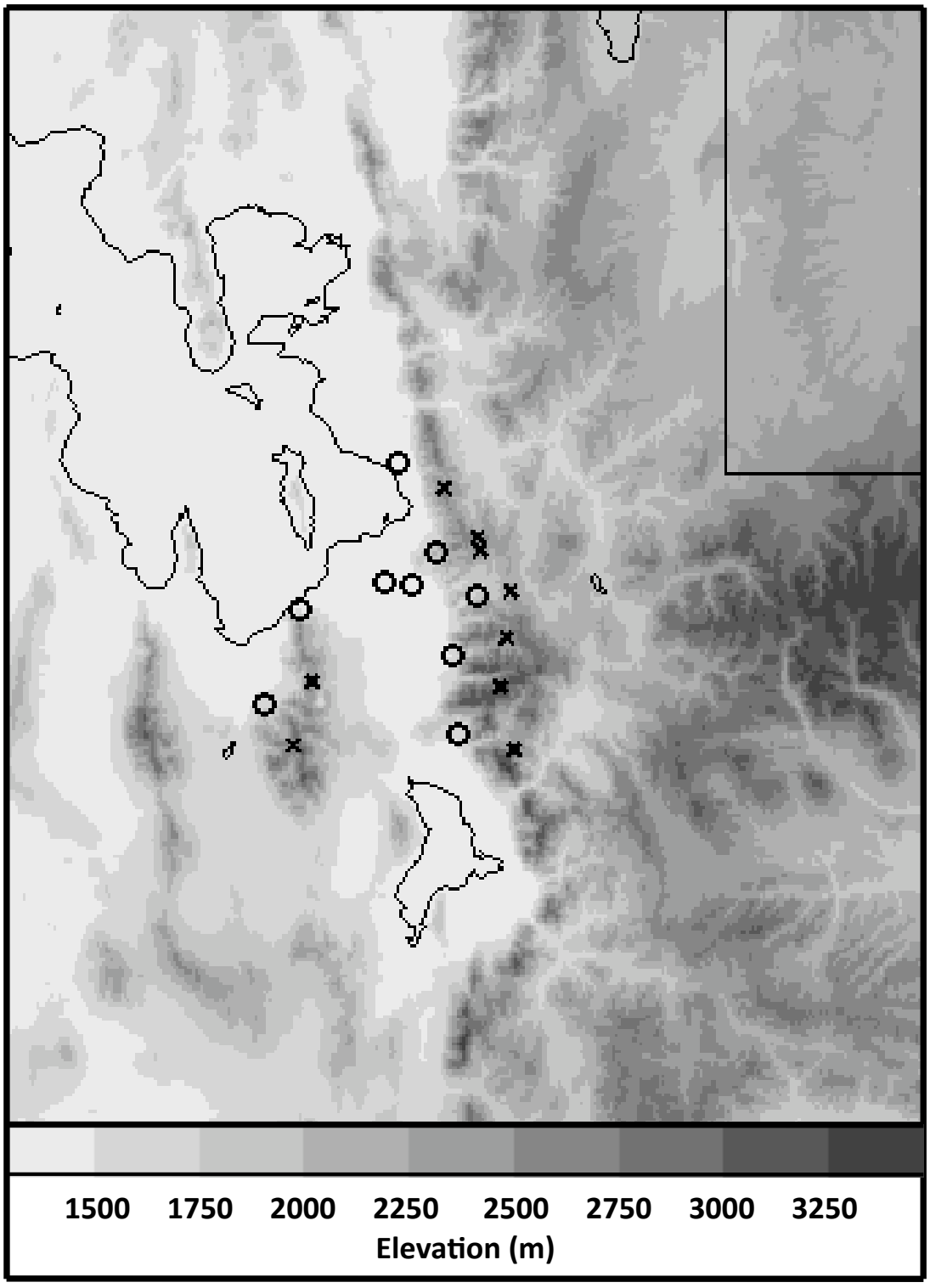


Figure 4.5. Map of surface stations used in COOP and SNOTEL lake-effect period fraction analysis. "o" indicates a COOP station. "x" indicates a SNOTEL station.

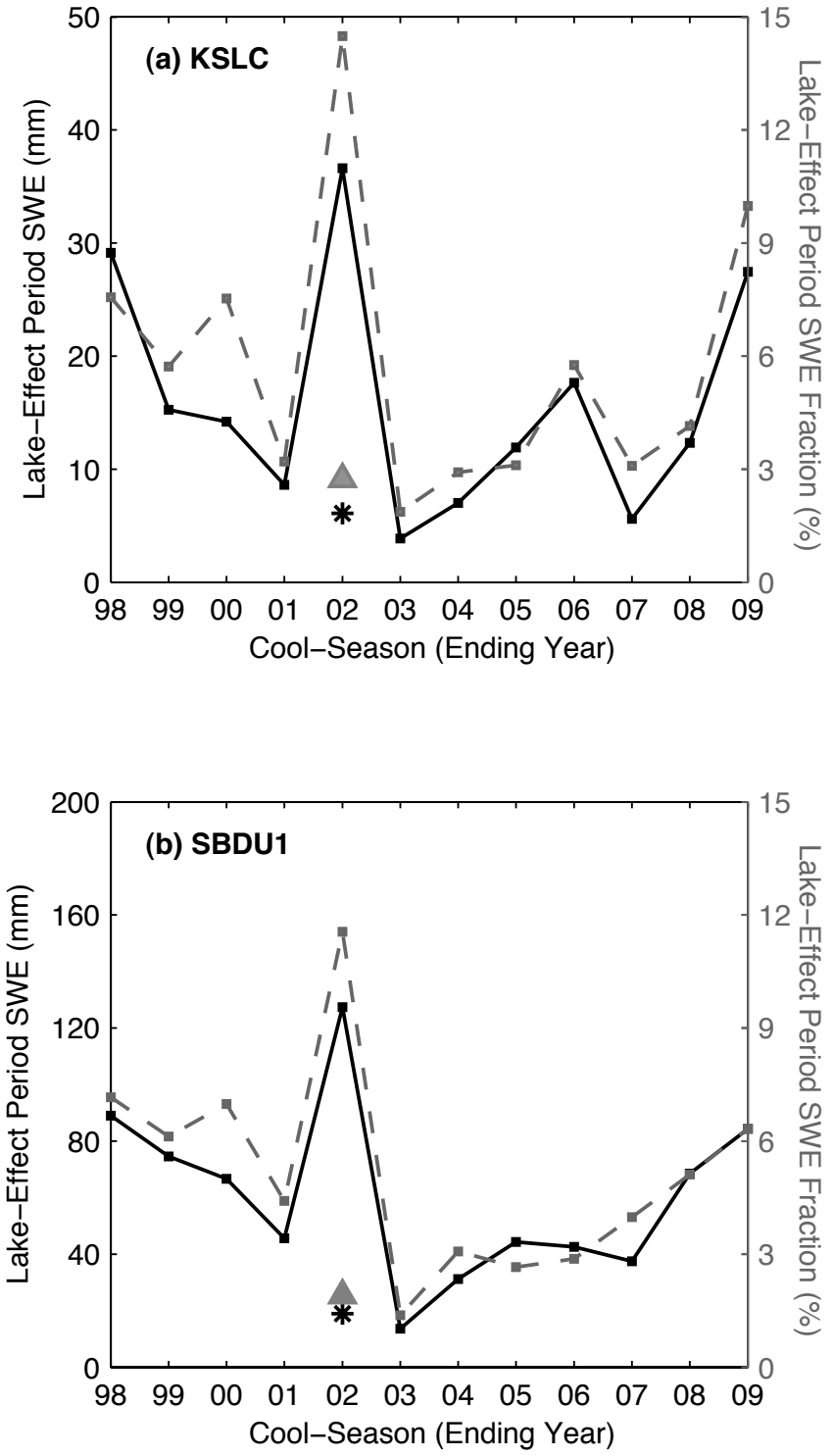


Figure 4.6. Cool-season lake-effect period SWE (mm, solid black line) and fraction (%, dashed grey line) at (a) KSLC and (b) SBDU1. Black asterisk and grey triangle indicate the lake-effect period SWE and fraction, respectively, after removal of the late Nov 2001 lake-effect periods described by Steenburgh (2003).

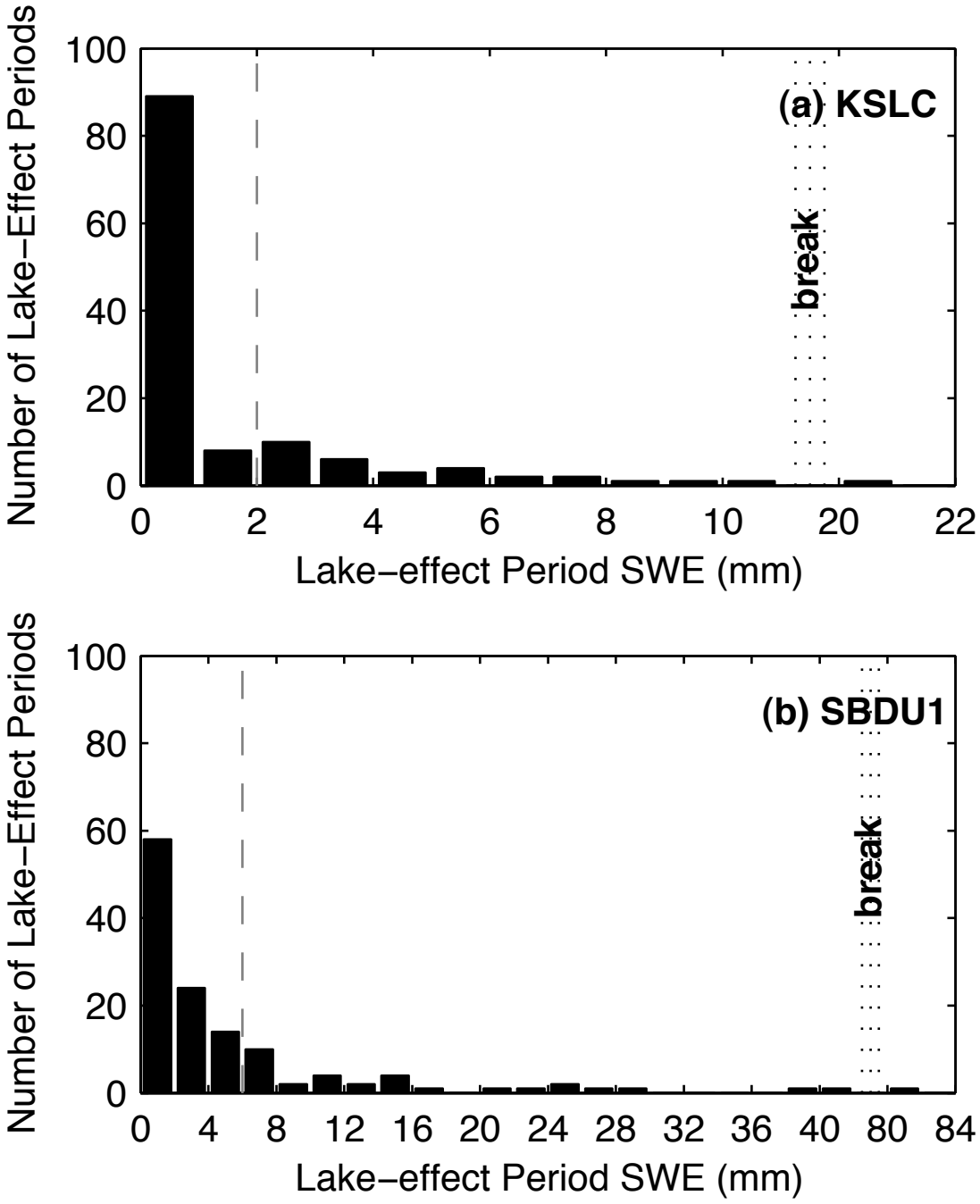


Figure 4.7. Frequency distribution of lake-effect period SWE (mm) by lake-effect period for (a) KSLC and (b) SBDU1. Grey dashed line shows the 75$^{th}$ percentile of lake-effect periods. Vertical dotted lines marked with a "break" indicate a break in the numbering on the x-axis.

periods of the hundred-inch storm results in a lake-effect period fraction of 2.7% at KSLC and 1.9% at SBDU1 during the 2001-2002 cool-season (grey triangle; Fig. 4.6a-b). A cumulative distribution function plot of lake-effect period SWE for KSLC and SBDU1 indicates that intense lake-effect periods like this are extremely infrequent (<1% probability of occurrence based on frequency during the study period), but have a profound impact on the overall lake-effect climatology (Fig. 4.8). A mere 12 lake-effect periods at KSLC and 13 lake-effect periods at SBDU1 account for 50% of the total accumulated lake-effect period SWE for the climatology (upper grey dashed line; Fig. 4.9a-b). Furthermore, 75% of the total accumulated lake-effect period SWE for the climatology comes from just 25 and 32 lake-effect periods at KSLC and SBDU1, respectively (lower grey dashed line; Fig. 4.9a-b).

The importance of episodic lake-effect periods is further demonstrated by the maximum lake-effect period SWE to fall in any given month during the study period (Fig. 4.10). At most stations, the amounts are substantially higher than the mean cool-season lake-effect period SWE (Fig. 4.11). Like the mean cool-season lake-effect period SWE, the largest monthly maximum lake-effect period SWEs are found at locations in the Oquirrh Mountains and Wasatch Mountains southeast of the GSL (Fig. 4.10). Collectively these results indicate that single lake-effect periods, or a sequence of lake-effect periods in a given month, play a dominant role in the lake-effect climatology.

## Monthly mean and variability

Mean monthly lake-effect period SWE exhibits a strong bimodal distribution (Fig. 4.12a-i). A primary peak occurs during Oct–Nov, a secondary peak in Mar–Apr, and a

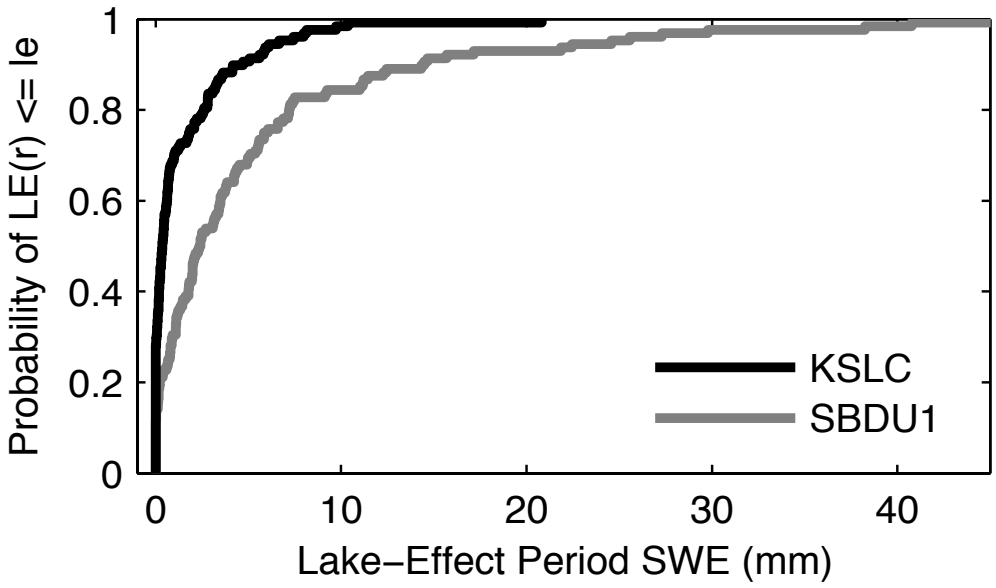


Figure 4.8. Cumulative distribution function (CDF) of lake-effect period SWE for all lake-effect periods identified in the climatology. The y-axis shows the probability that the lake-effect period SWE produced during a random lake-effect period [LE(r)] will be less than or equal to the amount of lake-effect period SWE (le) indicated by the x-axis.

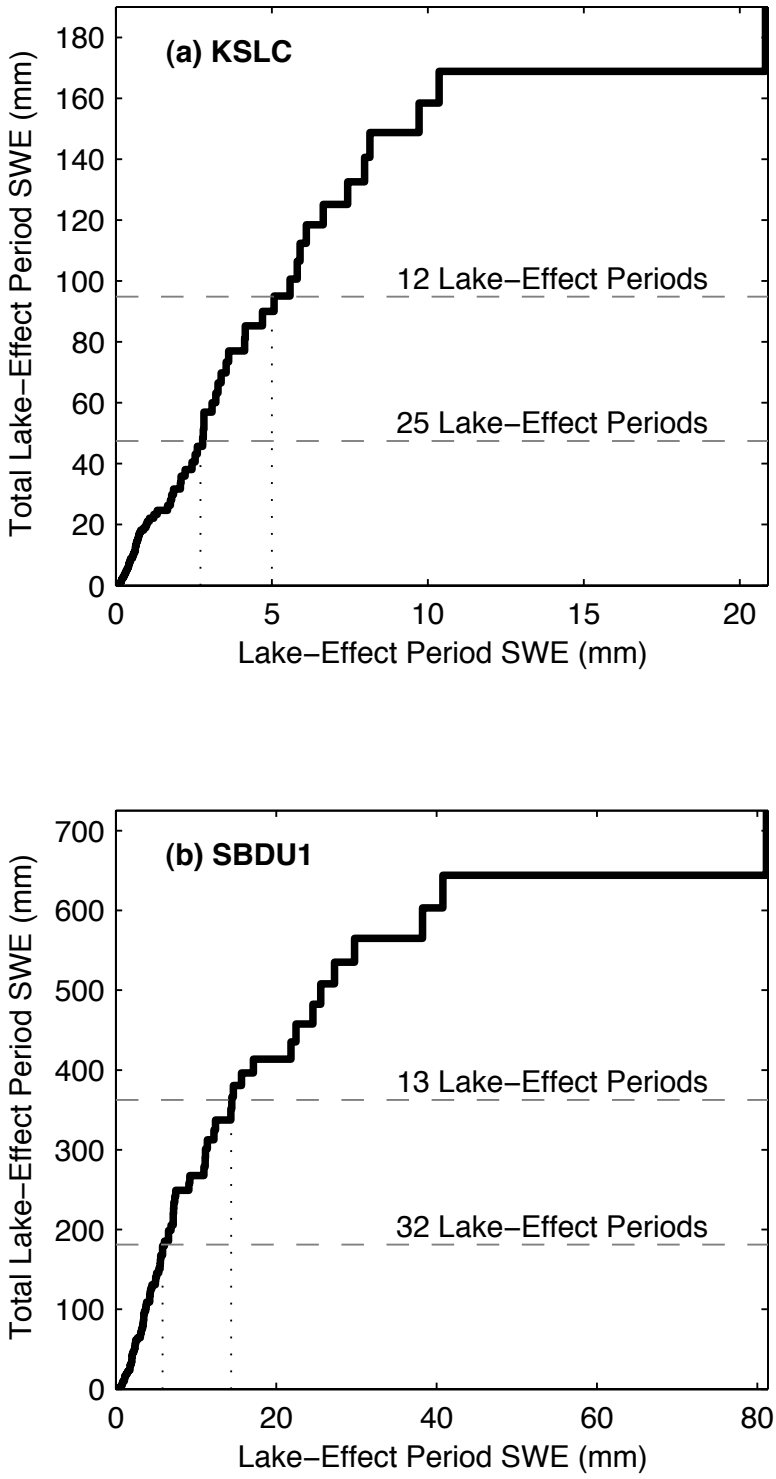


Figure 4.9. Lake-effect period SWE produced during single lake-effect periods vs. total accumulated lake-effect period SWE for the climatology for (a) KSLC and (b) SBDU1. Upper and lower grey dashed lines indicate the 25$^{th}$ and 50$^{th}$ percentiles of total accumulated lake-effect period SWE, respectively. The total number of lake-effect periods in the climatology is 128.

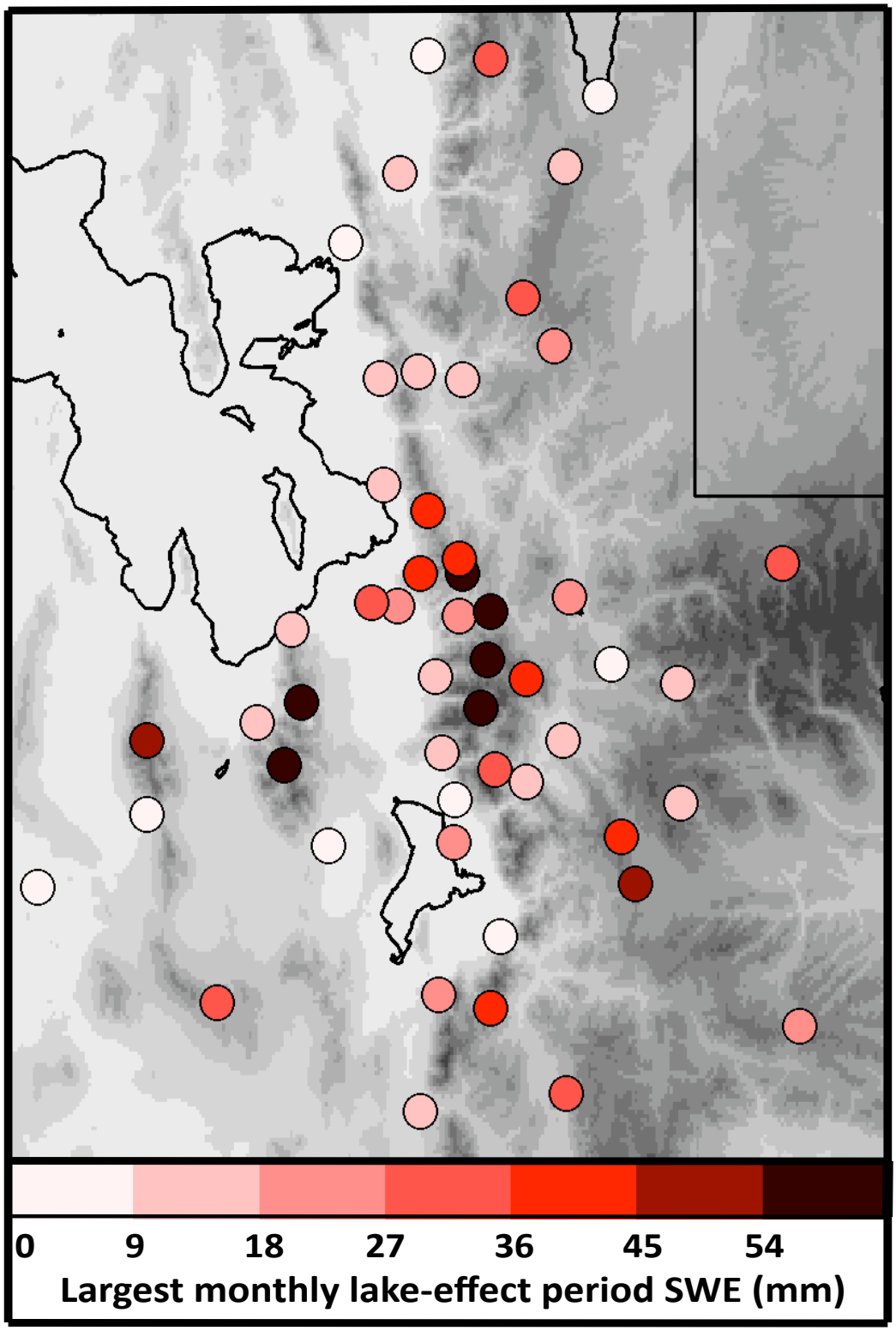


Figure 4.10. Largest monthly lake-effect period SWE (mm) during the study period. Maximum SWE is 119 mm.

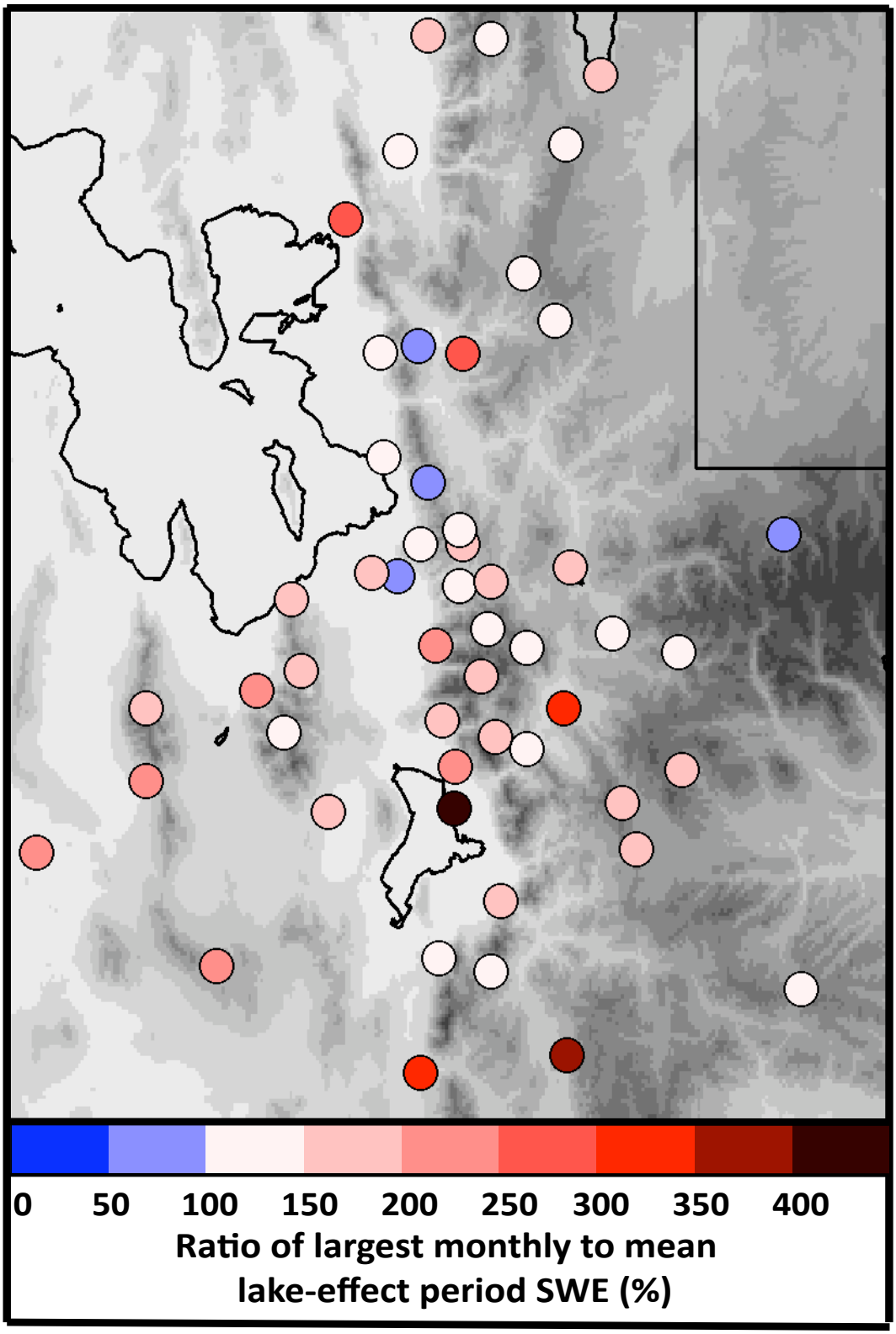


Figure 4.11. Ratio of largest monthly lake-effect period SWE to the mean cool-season lake-effect period SWE (%). Maximum is 665%.

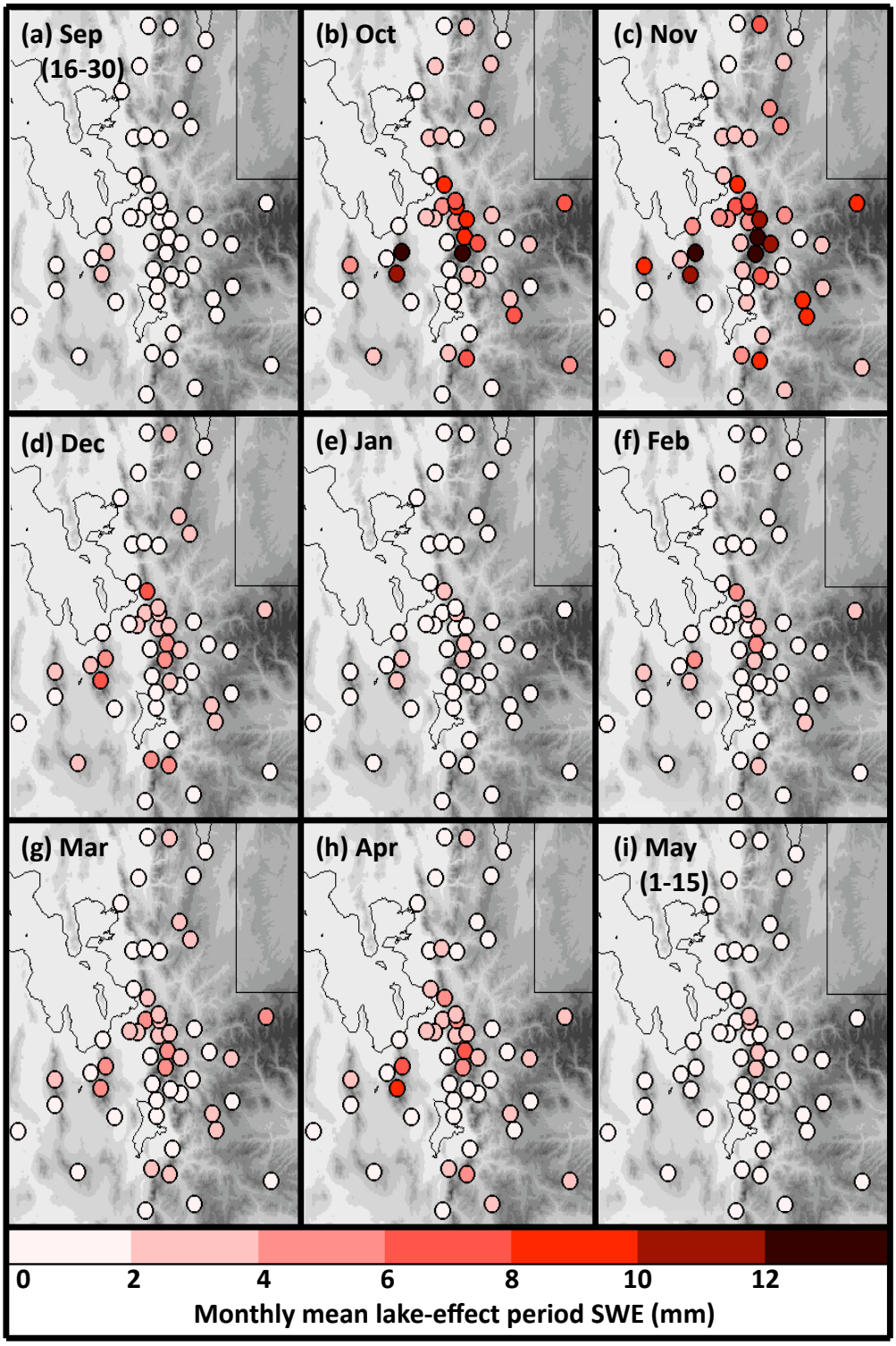


Figure 4.12. Monthly mean lake-effect period SWE (mm) for (a) Sep (16–30), (b) Oct, (c) Nov, (d) Dec, (e) Jan, (f) Feb, (g) Mar, (h) Apr, and (i) May (1–15). Maximum is 22.1 mm in Nov.

minimum in Jan–Feb. This bimodal distribution resembles that of the monthly frequency of lake-effect periods (Table 2.1; Alcott et al. 2012).

At KSLC, maxima in lake-effect period SWE occur in Nov and Apr (5.0 mm and 2.3 mm, respectively) and are separated by a Jan minimum (0.4 mm; Fig. 4.13a). SBDU1 exhibits a less pronounced bimodal distribution with lake-effect period SWE more heavily skewed towards the fall months. The fall peak occurs in Nov (22.1 mm) and a much less prominent spring peak occurs in March (5.4 mm; Fig. 4.13b). The winter minimum occurs in Feb (3.0 mm). Monthly lake-effect period amounts are much higher at SBDU1 than KSLC, again reflecting its mountainous location. At both locations, the Nov maximum is amplified by the lake-effect period SWE produced during the hundred-inch storm. Removing the SWE produced during these two lake-effect periods reduces the mean Nov lake-effect period SWE to 2.4 mm and 13.1 mm at KSLC and SBDU1, respectively (black asterisk in Fig. 4.13a-b), the former slightly less than the mean lake-effect period SWE in Oct.

## Environmental conditions

Forecasters commonly use the 700-hPa wind direction to determine which areas will receive the most intense SWE during a lake-effect period (Carpenter 1993; Steenburgh et al. 2000). Figure 4.14a-f presents the mean cool-season lake-effect period SWE for different 700-hPa wind directions. The most lake-effect period SWE occurs when the 700-hPa wind direction is between 300–330°, followed by 330–360° and 270–300° (Fig. 4.14b-d). The mean cool-season lake-effect period SWE is much lower for other flow direction, even at locations in the direct lee of the GSL. These results closely

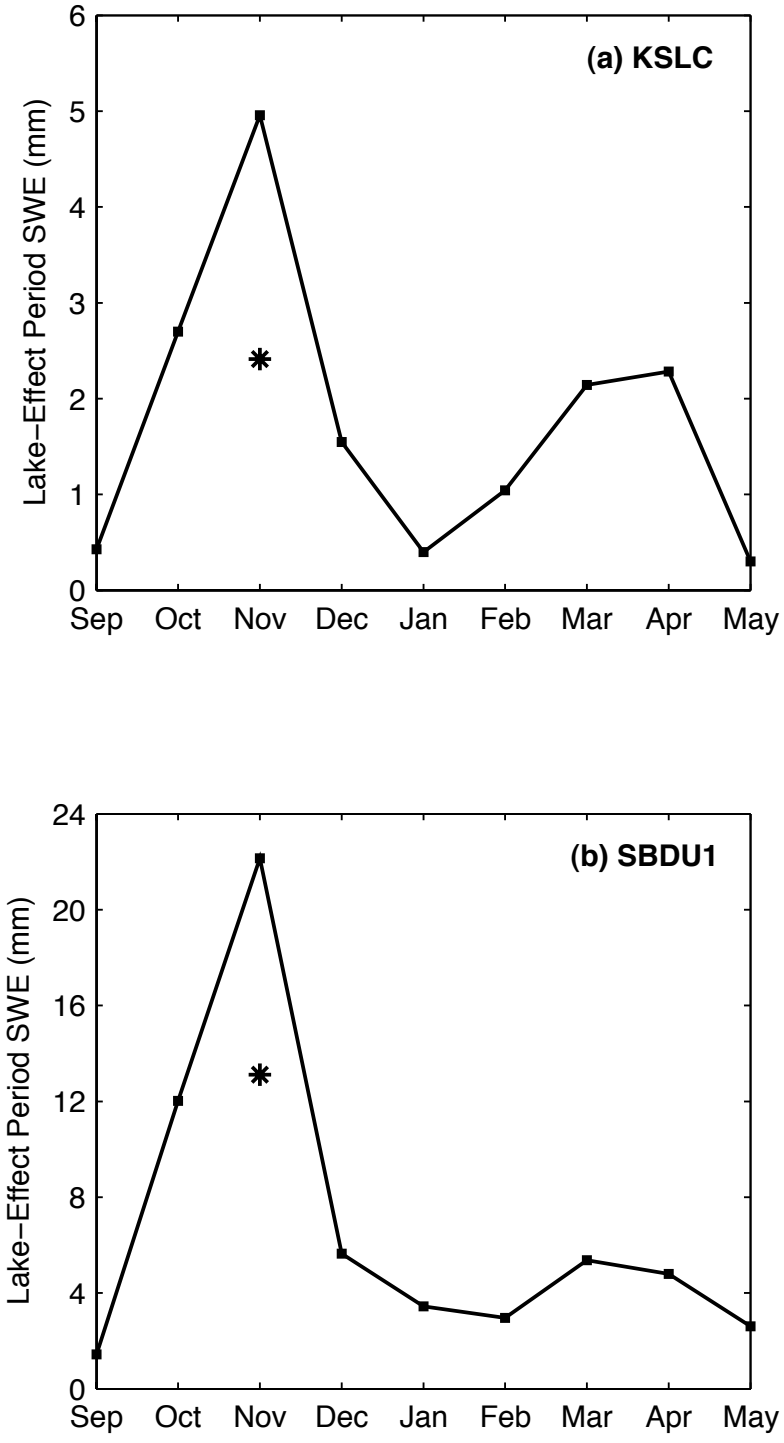


Figure 4.13. Mean monthly lake-effect period SWE (mm) for (a) KSLC and (b) SBDU1. Black asterisk indicates the lake-effect period SWE after removal of the late Nov 2001 lake-effect periods described by Steenburgh (2003).

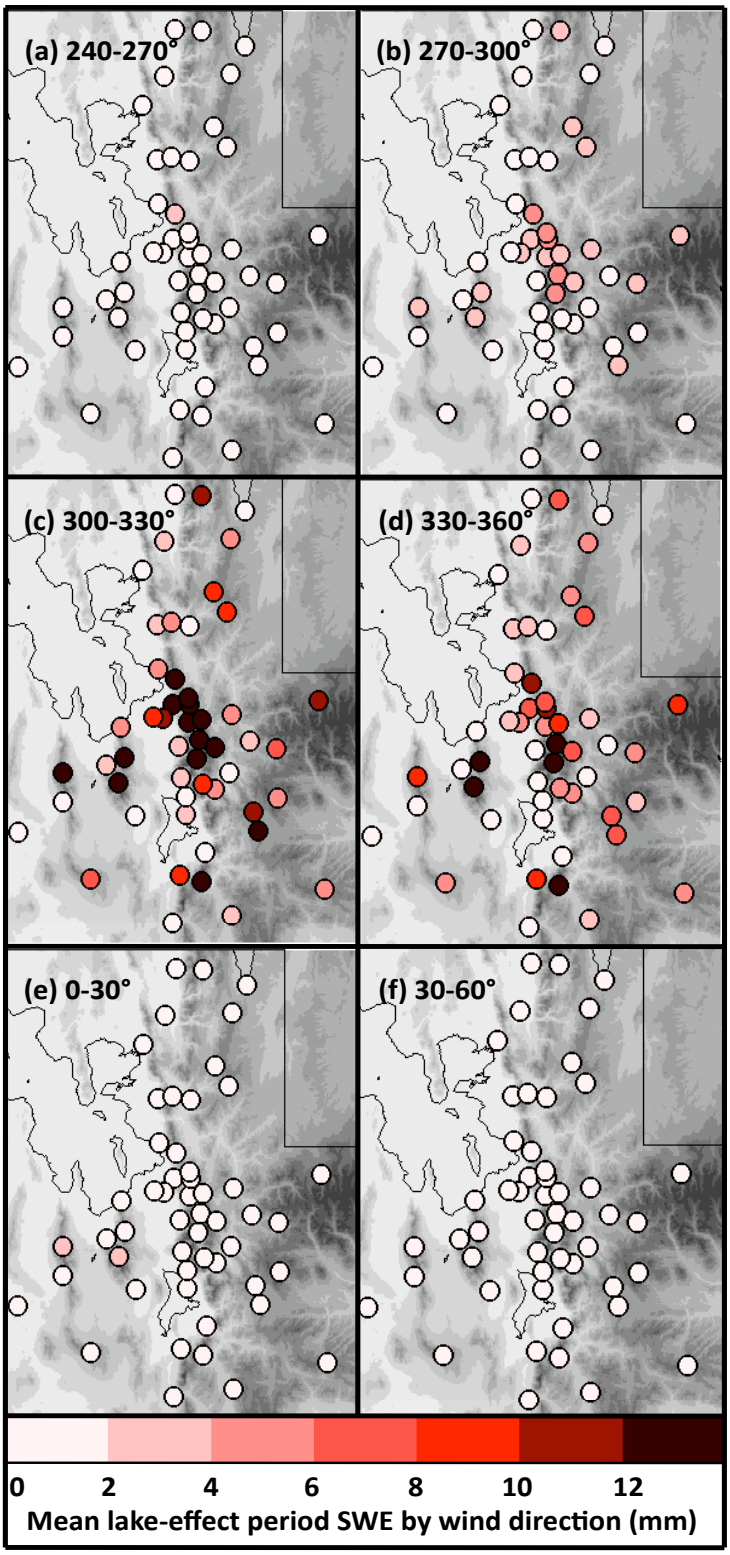


Figure 4.14. Mean lake-effect period SWE for 700-hPa wind directions between (a) 240-270°, (b) 270-300°, (c) 300-330°, (d) 330-360°, (e) 0-30°, and (f) 30-60°. Maximum is 32.0 mm when the 700-hPa wind is between 300-330°.

follow Alcott et al. (2012), who found that the majority (~70%) of lake-effect periods occur when the 700-hPa wind direction is between 300-360°, which features the greatest fetch across the GSL (Steenburgh et al. 2000).

A minimum lake-700-hPa temperature difference ($\Delta T$) of 16°C is also commonly used when forecasting lake-effect initiation (Steenburgh et al. 2000). However, Alcott et al. (2012) found that the threshold lake-700-hPa $\Delta T$ for lake-effect initiation is lower in the winter (as low as 12.4°C) and higher in the spring. Figure 4.15a-d shows mean cool-season lake-effect period SWE by lake-700-hPa $\Delta T$ exceedance, which is defined as the amount by which the observed lake-700-hPa $\Delta T$ surpasses the monthly-varying lake-700-hPa $\Delta T$ thresholds developed by Alcott et al. (2012). A strong signal does not exist between the lake-effect period SWE and the lake-700-hPa $\Delta T$ exceedance. Marginally more lake effect period SWE falls when the lake-700-hPa $\Delta T$ exceedance is between 0-2°C, whereas the lake-effect period SWE is similar for larger lake-700-hPa $\Delta T$ exceedance values.

Forecasters speculate that a correlation may exist between the area of the GSL and the frequency of lake-effect periods, however, Alcott et al. (2012) found no such correlation (Smart 2011). Figure 4.16a-b shows the standardized anomalies for lake-effect period SWE, GSL area, and 500-hPa trough days (defined later in the text), where the standardized anomaly is defined as the observation minus the mean divided by the standard deviation. Just like lake-effect period frequency, there is very little correlation between the area of the GSL and lake-effect period SWE at both KSLC and SBDU1 (correlation of 0.23 and 0.36, respectively).

Cool-seasons with fewer 500-hPa trough days, defined as a day when the 500-hPa

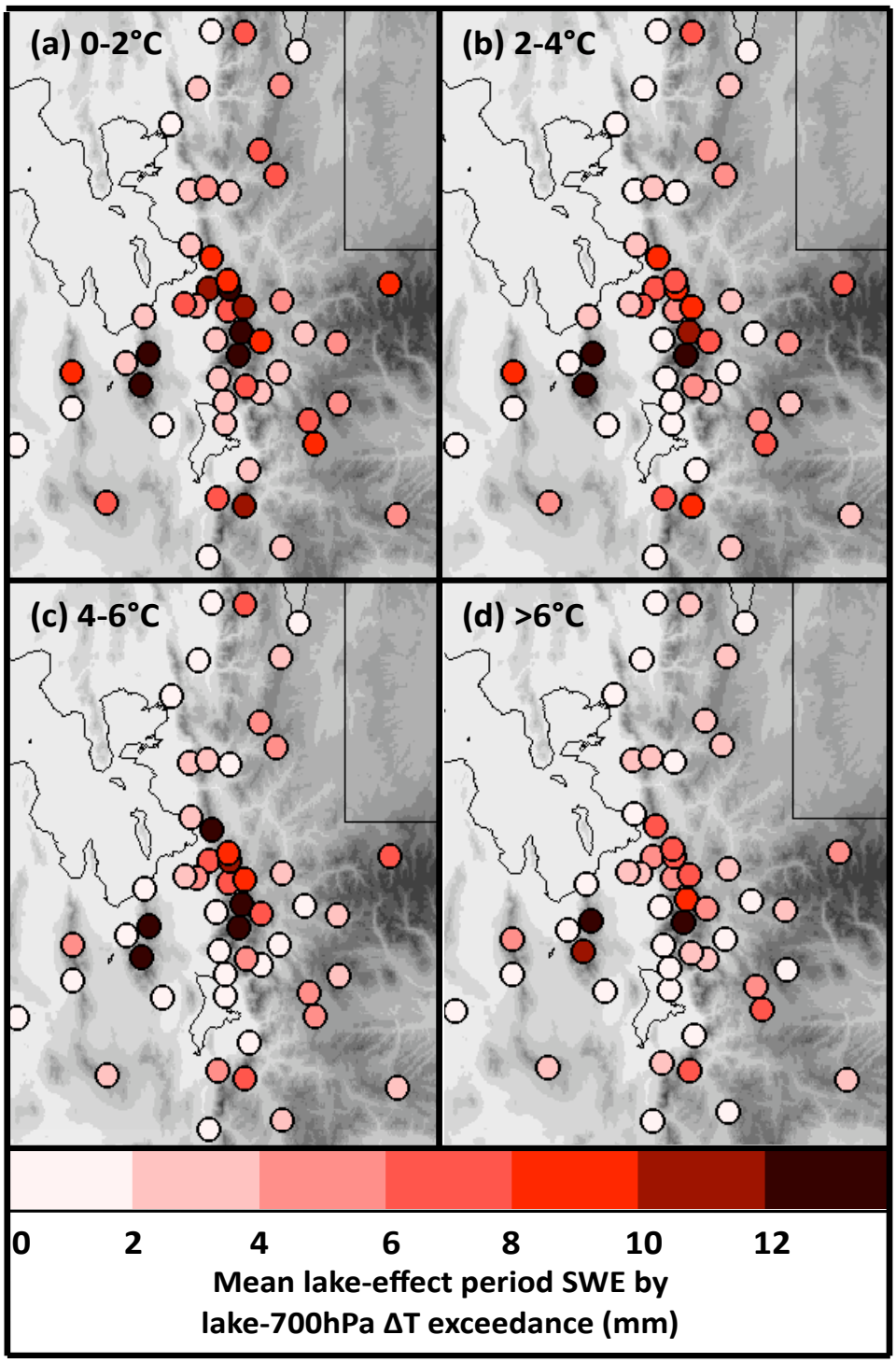


Figure 4.15. Mean lake-effect period SWE for lake-700-hPa $\Delta T$ exceedance between (a) 0-2°C, (b) 2-4°C, (c) 4-6°C, and (d) > 6°C. Maximum is 17.3 mm when the lake-700-hPa $\Delta T$ exceedance is between 0-2°C.

relative vorticity exceeds 2 x $10^{-5}$ $s^{-1}$, generally have fewer lake-effect periods (Alcott et al. 2012). However, there is almost zero correlation between lake-effect period SWE and the number of 500-hPa trough days at both KSLC and SBDU1 (correlation of 0.01 and 0.11, respectively; Fig. 4.16a-b). This suggests that the sample size is likely too small and too heavily influenced by episodic lake-effect periods to determine any clear relationship between lake-effect period SWE and associated synoptic features.

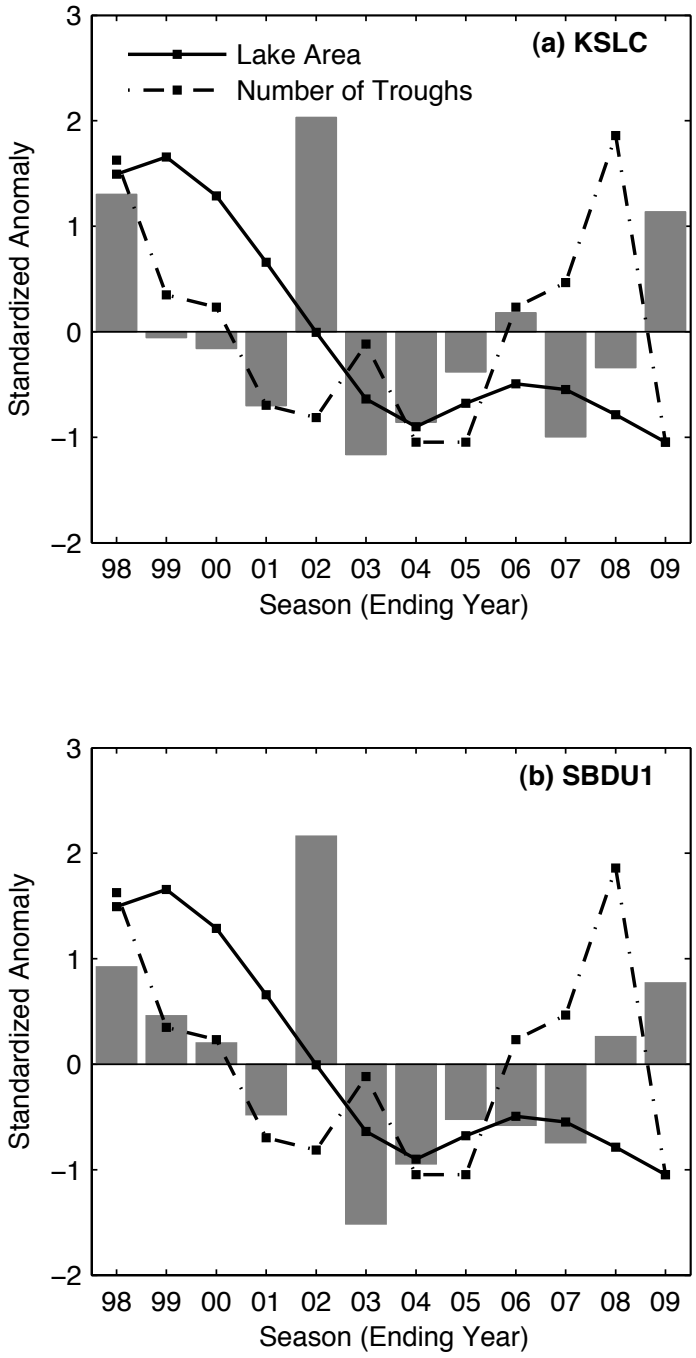


Figure 4.16. Standardized anomalies of cool-season lake-effect period SWE, GSL area, and the number of days with a trough at 500-hPa for (a) KSLC and (b) SBDU1.

# CHAPTER 5

# SUMMARY AND CONCLUSIONS

This thesis research developed and applied a method to quantify the amount of SWE produced during periods where GSLE can be subjectively identified by radar imagery. The method follows Wüest et al. (2010) and uses high temporal resolution radar-derived SWE estimates to disaggregate precipitation gauge observations from a daily to hourly time resolution. By combining the two datasets, we preserve the daily precipitation gauge totals and enable the separation of accumulated SWE into lake-effect and non-lake-effect periods.

The method was applied over 12 cool-seasons (1998–2009) encompassing 128 lake-effect periods and evaluated at two stations (KSLC and CLN) that are located in the lake-effect period SWE maximum southeast of the GSL. Evaluation at both stations indicates that the method works well for estimating climatological lake-effect period SWE totals. Scatter exists in the hourly SWE estimates, but the errors appear random and largely cancel when integrated over longer time periods. These errors likely arise from several sources including the comparison of volume and point measurements made by the radar and precipitation gauge, respectively, and the use of one Z-S relationship across all lake-effect periods. Furthermore, beam sampling issues including the overshooting of shallow storms, evaporation and sublimation below the lowest elevation radar scans, incomplete beam filling, and bright banding can contribute to Z-S errors.

The mean cool-season SWE produced during lake-effect periods (mean lake-effect period SWE) is greatest to the south and east of the GSL, coinciding with areas with the largest frequencies of occurrence of reflectivities greater than or equal to 10 dBZ. Large lake-effect period SWEs also occur in several areas well removed from the GSL including the Wasatch Mountains southeast of Utah Lake and the Bear River Mountains in northern Utah, demonstrating the other precipitation processes that can occur in tandem to GSLE. SNOTEL stations generally receive more lake-effect period SWE than COOP stations, reflecting both the mountainous locations of SNOTEL stations and a probable undercatch issue at unshielded COOP stations. Mean lake-effect period fractions (i.e. the mean cool-season lake-effect period SWE divided by the total cool-season SWE) are also greatest to the south and east of the GSL, but do not exceed 8.4%, indicating that the mean contribution of lake effect to cool-season SWE is modest.

Lake-effect period SWE and fraction are highly variable from season to season and can be heavily influenced by episodic lake-effect periods. Intense lake-effect periods are infrequent (averaging ~1 per cool-season), but have a profound impact on the overall climatology. Fifty percent of the total accumulated lake-effect period SWE for the climatology comes from just 12 lake-effect periods at KSLC and 13 lake-effect periods at SBDU1. Thus, care should be taken in interpreting mean values.

Mean monthly lake-effect period SWE exhibits a bimodal distribution with a primary peak in Oct–Nov and a secondary peak in Mar–Apr, closely resembling the monthly frequency of lake-effect periods as described by Alcott et al. (2012). Similarly, most lake-effect period SWE occurs when the 700-hPa wind direction is between 300–360°, corresponding to the 700-hPa wind direction with greatest frequency of lake-effect

periods and the longest fetch across the GSL.

On average, GSLE contributes modestly to the water budget of the GSL basin, though the contribution can vary greatly from cool-season to cool-season depending on the frequency and intensity of lake-effect periods. Cool-seasons with strong episodic lake-effect periods have a substantially larger contribution to the GSL basin water budget than those with only marginal lake-effect periods. Finally, the lake-effect period SWE quantified in this study is likely an overestimate because it includes SWE produced by all orographic, dynamical, and lake-effect processes occurring in concert during lake-effect periods. Thus, the average contribution of GSLE to the water budget of the GSL is likely *less* than the lake-effect period SWE presented in this thesis.

The method developed in this study has many other applications. It is an effective way to separate daily precipitation-gauge observations into smaller time resolutions, making it a potentially valuable resource for climatological precipitation studies. Great benefit would come from extending this climatology to include more cool seasons. This would give further insight to episodic GSLE periods, the parameters governing their intensity, and their impact on the overall climatology. Future work may also include isolating the disaggregation to stations residing below radar reflectivity returns directly corresponding to the lake-effect precipitation. This would require a spatial analysis of each radar scan during each lake-effect period, and would help filter out (but not eliminate) the SWE produced by other processes occurring alongside the lake effect. This would provide a more accurate estimate of the amount of SWE produced by GSL.

REFERENCES


Alcott, T. I., W. J. Steenburgh, and N. F. Laird, 2012: Great Salt Lake-Effect Precipitation: Observed Frequency, Characteristics and Associated Environmental Factors. For consideration in *Mon. Wea. Rev*.

Arnow, T., 1980. Water Budget and Water-Surface Fluctuations of Great Salt Lake. In: *Great Salt Lake: a scientific, historical and economic overview* (ed. By J. W. Gwynn) (Salt Lake City, UT), 255–264. Utah Geological and Mineral Survey.

Baer, V. E., 1991: The Transition from the Present Radar Dissemination System to the NEXRAD Information Dissemination Service (NIDS). *Bull. Amer. Meteor. Soc.*, **72**, 29–33.

Braham, R. R. and M. J. Dungey, 1984: Quantitative Estimates of the Effect of Lake Michigan on Snowfall. *J. Climate Appl. Meteor.*, **23**, 940–949.

Carlson, R. E., and J. S. Marshall, 1972: Measurement of Snowfall by Radar. *J. Appl. Meteor.*, **11**, 494–500.

Carpenter, D. M., 1993: The Lake Effect of the Great Salt Lake: Overview and Forecast Problems. *Wea. Forecasting*, **8**, 181–193.

Changnon, S. A., Jr., 1968: Precipitation Climatology of Lake Michigan Basin. Illinois State Water Survey Bulletin 52, Urbana, IL.

Crum, T. D., R. L. Alberty, and D. W. Burgess, 1993: Recording, Archiving, and Using WSR-88D Data. *Bull. Amer. Meteor. Soc.*, **74**, 645–653.

Daly, C. and Coauthors, 2007: Observer Bias in Daily Precipitation Measurements at United States Cooperative Network Stations. *Bull. Amer. Meteor. Soc.*, **88**, 899–912.

Doviak, R. J. and D. S. Zrnic, 1993: *Doppler Radar and Weather Observations*. Academic Press. 562 pp.

Eichenlaub, V. L., 1970: Lake Effect Snowfall to the Lee of the Great Lakes: Its Role in Michigan. *Bull. Amer. Meteor. Soc.,* **51**, 403–412.

Eischeid, J. K. and Coauthors, 2000: Creating a Serially Complete, National Daily Time Series of Temperature and Precipitation for the Western United States. *J. Appl. Meteor.*, **39**, 1580–1591.

Eltahir, E. A. B. and R. L. Bras, 1996: Precipitation Recycling. *Reviews of Geophysics*, **34**, 367–379.

Fujiyoshi, Y. and Coauthors, 1990: Determination of a Z-R Relationship for Snowfall Using a Radar and High Sensitivity Snow Gauges. *J. Appl. Meteor.*, **29**, 147–152.

Gorrell, M., 2011: Blue Skies Shine on Utah's Ski Season Openings. *Salt Lake Tribune*. [Available online at http://www.sltrib.com/sltrib/outdoors/52882948-117/ski-season-utah-brighton.html.csp].

Great Salt Lake Information System, cited 2011: Great Salt Lake Basin Watershed Description. [Available at http://www.greatsaltlakeinfo.org/Background/Description].

Greeney, C. M. and Coauthors, 2007: Winter test of production all-weather precipitation accumulation gauge for ASOS 2005–2006. [Available online at http://ams.confex.com/ams/87ANNUAL/techprogram/paper_116371.htm].

Groisman, P. Y., E. L. Peck, and R. G. Quayle, 1999: Intercomparison of Recording and Standard Nonrecording U.S. Gauges. *J. Atmos. Oceanic. Techol.*, **16**, 602–609.

Gunn, K. L. S. and J. S. Marshall, 1958: The Distribution with Size of Aggregate Snowflakes. *J. Meteor.*, **15**, 452–461.

Gwynn, J.W., 1980: *Great Salt Lake: a scientific, historical and economic overview*. Utah Geological and Mineral Survey. 480 pp.

Habib, E., G. J. Ciach, and W. F. Krajewski, 2004: A Method for Filtering out Raingauge Representativeness Errors from the Verification Distributions of Radar and Raingauge Rainfall. *Advances in Water Resources*, **27**, 967–980.

Hart, K. A. and Coauthors 2004: An Evaluation of Mesoscale-Model-Based Model Output Statistics (MOS) during the 2002 Olympic and Paralympic Winter Games. *Wea. Forecasting*, **19**, 200–218.

Kitchen, M. and R. M. Blackall, 1992: Representativeness Errors in Comparisons Between Radar and Gauge Measurements of Rainfall. *J. Hydrolo.*, **134**, 13–33.

Kuligowski, R. J., 1997: An Overview of National Weather Service Quantitative Precipitation Estimates. Techniques Development Laboratory Office Note 97-4. Silver Spring, MD.

Laird, N. F., J. Desrochers, and M. Payer, 2009: Climatology of Lake-effect Precipitation Events over Lake Champlain. *J. Appl. Meteor. Climatol.*, **48**, 232–250.

Lall, U. and M. Mann, 1995: The Great Salt Lake: A Barometer of Interannual Climatic Variability. *Water Resources Research*, **31**, 2503–2515.

—— and Coauthors, 1996: Nonlinear Dynamics of the Great Salt Lake: Nonparametric Forecasting. *Water Resources Research*, **32**, 975–985.

Mesinger, F. and Coauthors, 2006: North American Regional Reanalysis. *Bull. Amer. Meteor. Soc.*, **87**, 343–360.

Mohammed, I. N., D. G. Tarboton, 2011: On the Interaction Between Bathymetry and Climate in the System Dynamics and Preferred Levels of the Great Salt Lake. *Water Resources Research*, **47**, W02525.

National Weather Service, cited 2011: AWPAG Installation Dates for NWS and FAA owned ASOS sites. [Available online at http://www.nws.noaa.gov/asos/pdfs/AWPAG_stat.pdf].

—— , 1989: Cooperative Station Observations. National Weather Service Observing Handbook No. 2, Silver Spring, MD.

Natural Resources Conservation Service, cited 2011: SNOTEL and Snow Survey and Water Supply Forecasting. [Available online at http://www.wcc.nrcs.usda.gov/snotel/SNOTEL-brochure.pdf].

Ohtake, T. and T. Henmi, 1970: Radar Reflectivity of Aggregated Snowflakes. In: *Proc. 14th Radar Meteorology Conference* (ed. By Amer. Meteor. Soc.) (Tucson, Arizona), 209–210. Amer. Meteor. Soc.

Onton, D. J., W. J. Steenburgh, 2001: Diagnostic and Sensitivity Studies of the 7 December 1998 Great Salt Lake–Effect Snowstorm. *Mon. Wea. Rev.*, **129**, 1318–1338.

Paulhus, J. L. H. and M. A. Kohler, 1952: Interpolation of Missing Precipitation Records. *Mon. Wea. Rev*, **80**, 129–133.

Puhakka, T., 1975: On the Dependence of Z-R Relation on the Temperature in Snowfall. Preprints, *16th Radar Meteorology Conference* (ed. By Amer. Meteor. Soc.) (Houston, TX), 504–507. Amer. Meteor. Soc.

Rasmussen, R. and Coauthors, 2011: The Hotplate Precipitation Gauge. *J. Atmos. Oceanic Technol.*, **28**, 148–164.

—— and Coauthors, 2003: Snow Nowcasting Using a Real-Time Correlation of Radar Reflectivity with Snow Gauge Accumulation. *J. Appl. Meteor.*, **42**, 20–36.

—— and Coauthors, 2001: Weather Support to Deicing Decision Making (WSDDM): A Winter Weather Nowcasting System. *Bull. Amer. Meteor. Soc.,* **82**, 579–595.

Rinehart, R. E., 2004: *Radar for Meteorologists*. 4th ed. Rinehart Publications. 428 pp.

Salt Lake City Department of Public Utilities, 1999: Salt Lake City Watershed Management Plan. [Available online at http://www.slcgov.com/utilities/PDF%20Files/slcwatershedmgtplan.pdf].

Scott, R. W. and F. A. Huff, 1997: Lake Effects on Climatic Conditions in the Great Lakes Basin. *Illinois State Water Survey*, Champaign, IL.

Sekon, R. S. and R. C. Srivastava, 1970: Snow Size Spectra and Radar Reflectivity. *J. Atmos. Sci.*, **27**, 299–307.

Serreze, M. C., M. P. Clark, and R. L. Armstrong, 1999: Characteristics of the western United States snowpack from snowpack telemetry (SNOTEL) data. *Water Resources Research*, **35**, 2145–2160.

Sieck, L. C., S. J. Burges, and M. Steiner, 2007: Challenges in obtaining reliable measurements of point rainfall. *Water Resources Research*, **43**, W01420, 23 pp.

Smart, C., 2011: Boats and Birds to Benefit from Rising Great Salt Lake. *Salt Lake Tribune.* [Available online at http://www.sltrib.com/sltrib/news/51961865-78/lake-salt-according-bird.html.csp].

Steenburgh, W. James, Trevor I. Alcott, 2008: Secrets of the "Greatest Snow on Earth". *Bull. Amer. Meteor. Soc.*, **89**, 1285–1293.

——, 2003: One Hundred Inches in One Hundred Hours: Evolution of a Wasatch Mountain Winter Storm Cycle. *Wea. Forecasting*, **18**, 1018–1036.

—— and D. J. Onton, 2001: Multiscale Analysis of the 7 December 1998 Great Salt Lake–Effect Snowstorm. *Mon. Wea. Rev.*, **129**, 1296–1317.

——, S. F. Halvorson, and D. J. Onton, 2000: Climatology of Lake-Effect Snowstorms of the Great Salt Lake. *Mon. Wea. Rev.*, **128**, 709–727.

Tokay, A., P. G. Bashor, and V. L. McDowell, 2010: Comparison of Rain Gauge Measurements in the Mid-Atlantic Region. *J. Hydrometeor*, **11**, 553–565.

United States Geological Survey Utah Water Science Center, cited 2011: Great Salt Lake. [Available at http:..ut.water.usgs.gov/greatsaltlake/].

Vasiloff, S. V., and Coauthors, 2007: Improving QPE and Very Short Term QPF., *Bull. Amer. Meteor. Soc.*, **88**, 1899–1911.

Vasiloff, S., 2001: WSR-88D Performance in Northern Utah during the winter of 1998–1999. Part I: Adjustments to Precipitation Estimates. Western Regional Technical Attachment NO. 01-03, Salt Lake City, Utah.

Wallis, J. R. and Coauthors, 2007: Regional Precipitation-Frequency Analysis and Spatial Mapping for 24-hour and 2-hour Durations for Washington State. *Hydrology and Earth System Sciences*, **11**, 415–442.

Warning Decision Training Branch, cited 2011: WSR-88D Winter Weather Precipitation Estimation. [Available online at http://www.wdtb.noaa.gov/courses/winterawoc/IC7/lesson2/part1/player.html].

Western Regional Climate Center, cited 2011: Utah Climate Summaries. [Available at http://www.wrcc.dri.edu/summary/climsmut.html].

Westrick, K. J., C. F. Mass, and B. A. Colle, 1999: The Limitations of the WSR-88D Radar Network for Quantitative Precipitation Measurement over the Coastal Western United States. *Bull. Amer. Meteor. Soc.*, **80**, 2289–2298.

Wüest, M. and Coauthors, 2010: A Gridded Hourly Precipitation Dataset for Switzerland Using Rain-Gauge Analysis and Radar-Based Disaggregation. *Inter. J. Climatol.*, **30**, 1764–1775.

Young, K. C., 1992: A Three-Way Model for Interpolating for Monthly Precipitation Values. *Mon. Wea. Rev.*, **120**, 2561–2569.